STRUCTURE AND REACTIVITY OF NANOSTRUCTURED MATERIALS AND THEIR METAL COMPLEXES WITH CO MOLECULES

INTRODUCTION

Heterogeneous catalysis is of crucial importance for the chemical industry; the number of heterogeneous catalysts applied in industry is very large and they come in many different forms. There are some common forms that have been widely used in practical applications such as transition metals, metal oxides, zeolites and clay. Among those types of catalysts, metal oxide surface as an example of 2 dimensional heterogeneous catalysts while zeolite is very fascinating for being a representative of 3 dimensional heterogeneous catalysts.

Zeolite is a type of crystalline aluminosilicate found in nature in several different structures. It has been used daily as a high-potential catalyst in many industrial reactions. The active site takes place in a zeolite structure when any framework silicon atom is replaced by an aluminum atom. A Brønsted acid site, a Lewis exchanged-metal cation site or other type of active site could occur to compensate for the negative charge from Al substitution. These active sites play a key factor in its catalytic property. Other factors generally come from the unique structure of zeolite and its well-defined pores and channels. Zeolites have empty space (cavities or channels) that can host cations, water, or other guest molecules (Figure 1). Many studies have been focused on this kind of catalyst to figure out factors that affect such catalytic properties. This knowledge is necessary for developing new types of zeolites.

Despite the advances in experimental techniques and instruments, knowledge about those heterogeneous catalysts is still far from being clearly understood. The main reason is the complexity in the catalysts' structures. Moreover, because of their bulky framework, characterization of the active site is still difficult. Even though some experimental techniques can give some limited insights, there remain many questions. Theoretical method is an elegant way to get more understanding of such systems. Many theoretical models have been proposed to study condensed phase systems. The bare cluster methodology treats the active part, including the relevant region, and the adsorbate by quantum mechanics as an isolated system while entirely ignoring the effects of the remaining crystal framework. Electronic and catalytic properties of the active site are significantly influenced by the lattice thus the finite cluster approach has failed to describe such a system as a result of not taking into account for the periodicity.

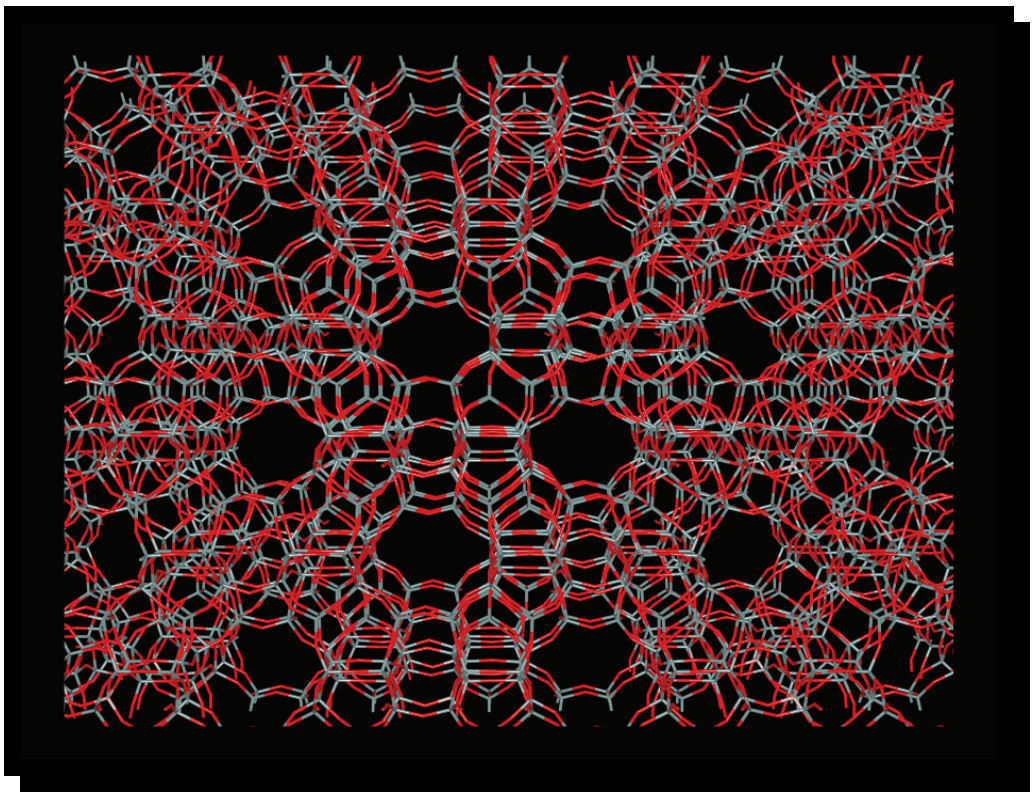

Figure 1 The framework of ZSM-5 zeolite composed of well-defined pores and channels where water or guest molecules can occupy.

In the face of rapid advances in computer technology and the great efforts being made towards improving the efficiency of electronic structure methods, modeling reactivity in extended systems remains a challenge for quantum chemistry. Many periodic electronic structure methods, such as periodic Hartree-Fock and periodic DFT, are available for providing an accurate framework to model interactions in extended systems such as crystals or surfaces. A number of periodic density functional theory studies of interactions on small surface systems (Hill *et al.*, 1999; Jeanvoine *et al.*, 1998; Larin and Vercauteren, 2001; Shah *et al.*, 1997; Sierka and Sauer, 2001; Teunissen *et al.*, 1994a) have been reported (<100 atoms/unit cell). These periodic DFT calculations used massive computational resources even for small periodic systems. However, most zeolites have very large unit cells (>100 atoms/unit cell) and also we need a large super-cell to provide a good description for metal oxide, and thus accurate results cannot be achieved practically even with current day resources.

Another sophisticated computational method often employed is the embedded cluster method. There is sufficient support from previous works that, in the case of extended systems, the effects of the remaining crystal lattice, mainly the Madelung potential, are crucial for obtaining quantitative understanding of the mechanisms of chemical processes that occur at the active sites (or defects) of the crystal. The embedded cluster methodology takes advantage of the simplicity of the cluster approach, but adds the effects of the crystal framework in an approximate manner. The electronic embedding approach accounts for the static electrostatic Madelung potential from the crystal framework and includes its effects directly in the Fock matrix elements of the quantum cluster; thus its wave function is polarized. Two approximations known as the electronic embedding and the mechanical embedding approaches have been developed. The major part of lattice effects is the electrostatic potential from periodic lattice which is called the Madelung potential. The easiest way to represent the Madelung potential is to embed the quantum cluster in an array of point charges representing the electrostatic potential from the outer part. Several methods have been proposed to produce the fictitious point charges surrounding the cluster. To include all other effects, a quantum cluster could be incorporated with a

molecular mechanics force field, called the QM/MM model. The force field can be fitted to experimental data or any calculation results. The reliability of this approach depends on the quality of the force field. Moreover, the more general combined method named ONIOM (our Own N-layered Integrated molecular Orbital and molecular Mechanics) is widely employed as well. Although they have inherent fundamental approximations, those approaches have been shown to perform quite well for many studies on adsorption and reactions at the active sites of zeolites.

Furthermore, not only zeolites but carbon nanomaterials are very interesting and widely acknowledged as being feasible for several groups of applications. Initially, they have proved to be of great benefit in mechanical utilization due to their astonishing hardness and weightlessness properties. They have also been targeted for numerous potential applications, including electronic device components (Collins and Avouris, 2000; Franklin *et al.*, 2002; Rotkin and Zharov, 2002), hydrogen storage media (Cao *et al.*, 2001; Li *et al.*, 2003; Pan *et al.*, 2005), and novel nanoscaled biosensors (Gooding, 2005; Lin *et al.*, 2004; Sotiropoulou and Chaniotakis, 2003; Wohlstadter *et al.*, 2003).

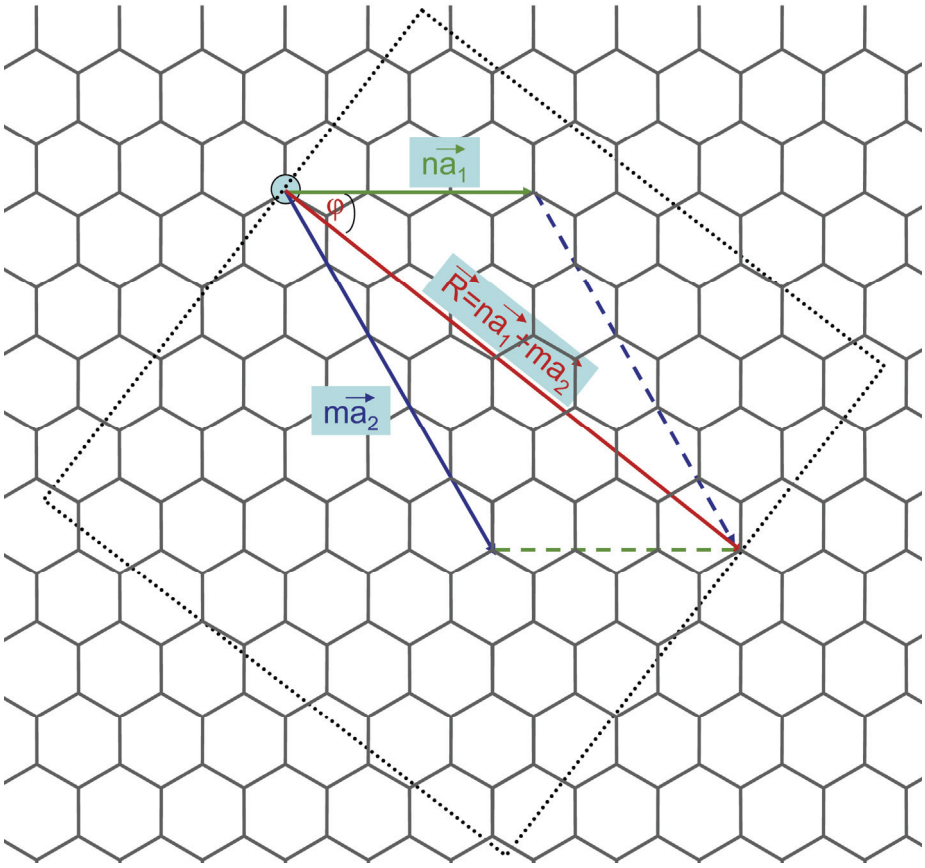

Figure 2 Flat hexagon lattices of a graphene sheet showing the chiral vector R and the wrapping angle φ.

Fundamentally, carbon nanotubes exist as a macro-molecule of carbon, analogous to a sheet of graphite rolled into a cylinder. Graphite looks like a sheet of honey comb, a tessellation of hexagonal rings of carbon. Sheets of graphite lay stacked on top of one another, but they slide past each other and can be separated easily, which is how it is used for writing. However, when coiled, the carbon arrangement becomes very strong. In fact, nanotubes have been known to be up to one hundred times as strong as steel and almost two millimeters long. These nanotubes have a hemispherical "cap" at each end of the cylinder. They are light, flexible, thermally stabile, and are chemically inert. They have the ability to be either metallic or semi-conducting depending on the "twist" of the tube.

Nanotubes form different types, which can be described by the chiral vector (n, m), where n and m are integers of the vector equation $R = na_1 + ma_2$. The chiral vector is determined by the Figure 2. The vector a_1 lies along the zigzag line. The other vector a_2 has a different magnitude than a_1, but its direction is 60° to the vector a_1. When added together, they equal the chiral vector R. The wrapping angle φ is formed between R and the Zigzag line. If R lies along the Zigzag line (φ =0° or 60°), then it is called a "Zigzag" nanotube. If φ=30°, then the tube is of the "Armchair" type. Otherwise, it is a "chiral" tube. The values of n and m determine the chirality, or "twist" of the nanotube. The chirality in turn affects the conductance of the nanotube, its density, its lattice structure, and other properties. A SWNT is considered metallic if the value n - m is divisible by three. Otherwise, the nanotube is semiconducting. Consequently, when tubes are formed with random values of n and m, we would expect that two-thirds of nanotubes would be semi-conducting, while the other third would be metallic.

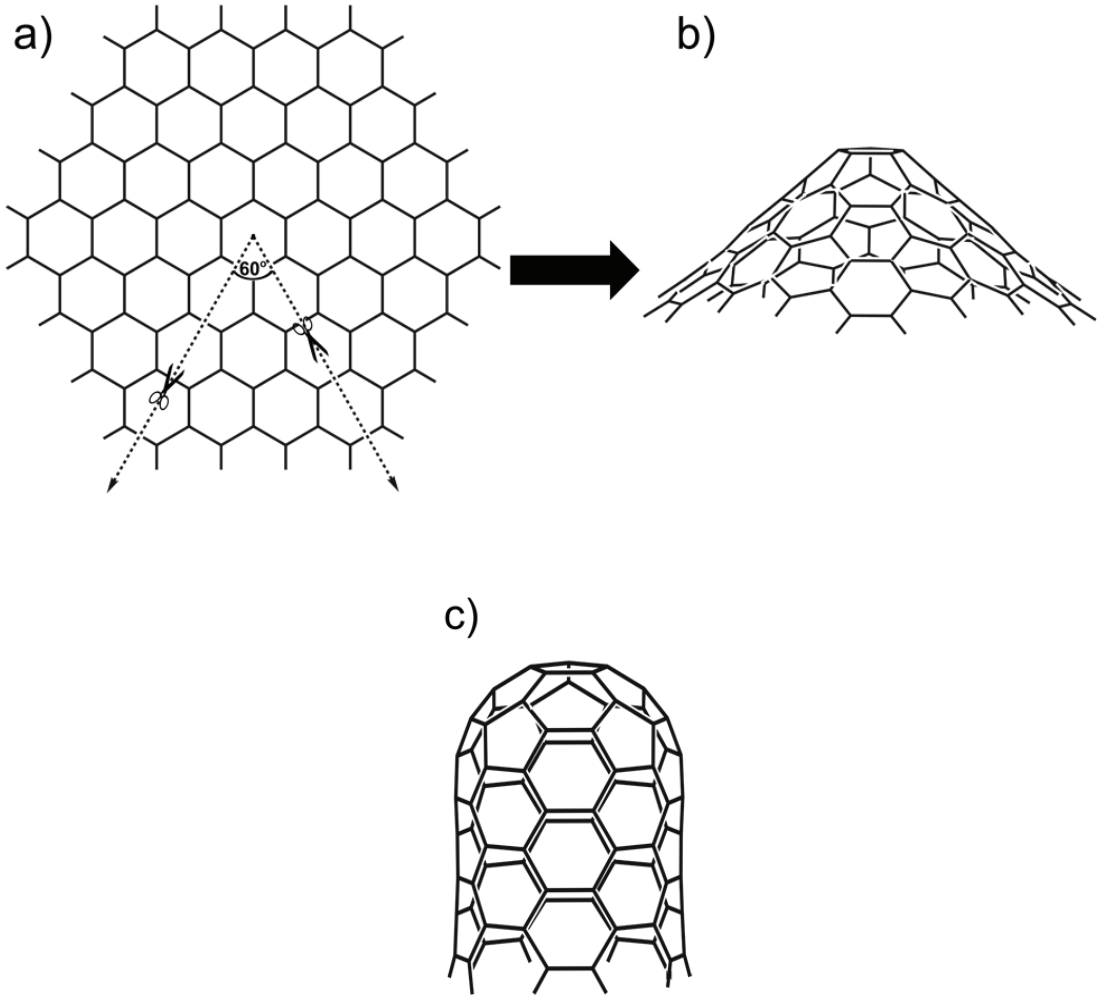

Figure 3 Through slicing of graphene sheet (a) by 60^{o} disclination angle and roll up, one could construct the conical tip (b) of a single wall carbon nanohorn where the top region part is similar to that of the encapsulated single wall carbon nanotube (c).

An interesting aspect of carbon nanotubes is that a number of topological defects, such as the pentagon in the hexagonal carbon lattice leading to a formation of conical shape, can occur near the capped end of the carbon nanotube. A conjunction of this nanocone and cylindrical carbon cluster is recognized as the single-wall carbon nanohorn (SWNH).

A conic carbon cluster, which is a tip of carbon nanohorn, could be simplified as a structure with fivefold symmetry that forms due to a 60^{o} disclination defect in a two-dimensional graphene sheet (cf. Figure 3). The arrangement of carbon atoms (20 atoms) at the apex of the conical carbon nanohorn tip is analogous to the fullerene hemisphere at the end of the encapsulated carbon nanotube. Both carbon nanohorns and carbon nanotubes show the capability to be candidates for such applications in drug delivery, energy storage or minute-scale sensors (Ajima *et al.*, 2005).

In this thesis, I have focused on utilizing an embedded cluster approach called SCREEP model (Stefanovich and Truong, 1998), a finite quantum cluster is embedded in a potential field generated by sets of point charges representing the Madelung potential from periodic structure, to represent the complicated extended systems such as zeolites. This method is applied to systems of interest to examine the advantages and disadvantages of the methods. In one system, the adsorptions of CO in H-ZSM-5 and Li-ZSM-5 zeolites have been studied. Furthermore for comparison between the reactivity of active site in difference types of zeolites, the interactions of CO in H-FAU and Li-FAU zeolites have been investigated and compared along with those in ZSM-5 zeolite models.

In another system, the adsorption of CO and NO on Ag-ZSM-5, which is considered to be the first step of the NOx decomposition reaction catalyzed by Ag-ZSM-5, has been studied. Although this process has been utilized on an industrial scale to reduce toxic gases emitted from industry, the mechanism and the suitable conditions for this reaction are still unclear. This would provide us a better

understanding of the consequence of the crystal effects in the study of zeolite. The results of this study are important for establishing a cost effective methodology for future studies on the mechanisms of metal exchanged-zeolites and also other extended systems.

In addition, I also want to comprehend the difference between the properties of the single-wall carbon nanohorn and the single-wall carbon nanotube tips by means of the rigorous, reliable density functional theory (DFT) method. In order to ascertain the most favorable site for the gold atom, nine positions among the analogous region of SWNH and SWNT tips were taken into consideration. To observe the property of the gold atom on different supporting materials, a carbon monoxide molecule was used as a probe molecule for investigating and comparing the reactivity of the gold atom on the tips of both the carbon nanohorn and carbon nanotube.

LITERATURE REVIEW

Zeolites provide a versatile class of shape-selective catalysts for important chemical processes such as petroleum cracking and reforming. Catalytic processes in zeolites are activated by active sites which are the Brønsted acid site and the ion exchanged Lewis acid site. However, not only the active sites but unique pores and channels in the zeolite framework also play an important role on catalytic properties of zeolite. There are several studies on zeolite in both experimental and theoretical methods. Theoretical approaches are very helpful for providing information at the molecular electronic level.

Owing to the bulkiness and complexity of zeolite structures, extraordinary conducting technique methods are essential in a study of the properties or reactions occurring inside zeolite. A small cluster model, which comprises only the reactive center while neglecting the remaining zeolite structure, is frequently used. However, many reports infer that such environment effects are significant and, in addition some serious errors may arise (Boronat *et al.*, 2001; Hill *et al.*, 1999; Khaliullin *et al.*, 2001; Limtrakul *et al.*, 2001; Martinez-Magadan *et al.*, 2002; Rozanska *et al.*, 2001; Sinclair *et al.*, 1998; Zygmunt *et al.*, 2000). Furthermore, as a consequence of ignoring long-range forces and some hydrogen bonding, small clusters lack the steric constraints that characterize adsorption in zeolites. In effect, the cluster has insufficient influence on the zeolitic cavity to activate confinement effect. Several techniques can be considered for solving the problems of small cluster models. The simplest way is to use progressively larger clusters until the desired properties converge (Gonzales *et al.*, 1997; Zygmunt *et al.*, 2000). It is clear that with increasing the cluster size, the important local electronic and steric effects are included, while the effect of the terminating region becomes smaller since it is further separated from the reaction site.

There are further promising ways for including long-range forces, for instance periodic quantum calculations (Civalleri *et al.*, 2001; Kresse and Furthmueller, 1996; Shah *et al.*, 1996) and embedded clusters (Greatbanks *et al.*, 1994; Maseras and

Morokuma, 1995; Sierka and Sauer, 2000). The periodic approach, which is typically based on the density functional theory (DFT), is relatively straightforward and provides the only reliable method for testing approximations other than those in DFT itself (Astala and Auerbach, 2004; Astala *et al.*, 2004). However, in the present circumstance, periodic DFT calculations suffer from the main disadvantage that they are expensive, treating all atoms equally, even distant spectator atoms; and they can be applied only to zeolites with sufficiently small unit cells. In most practical zeolites, the unit cells are substantially large, such as 288 atoms for the ZSM-5. Therefore, the accurate periodic electronic structure methods are rather impractical.

The embedded cluster methodology takes advantage of the simplicity of the cluster approach but adds the effects of the crystal framework in an approximated manner. The general idea involves breaking a total system (S) into an inner region (I) of chemical interest and an outer environment (O). For zeolites and other covalent-network solids, this partitioning inherently leaves dangling bonds requiring special methods to saturate the bonding in I. Typically link atoms are added to the inner region, yielding a cluster (C). One then simulates the cluster C with high chemical accuracy (high), while modeling region O with much cheaper methods (low). If a cluster is large enough, the short- and medium-range (local) interactions between the active region and its environment are just about completely included. Only the long-range interaction from the extended framework is concerned as the lattice effect. The major component of lattice effects is the Madelung potential which can be taken into account by means of electronic embedding calculation. This approach provides the static electrostatic Madelung potential from the crystal framework and applies such effects directly in the Fock matrix elements of the quantum cluster, thus the wave function is polarized. The crystal polarization and long-range structure relaxation, normally considered to be insignificant, are typically abandoned in electronic embedding methods. This type of embedding method has been proved to be adequate for a dominant fraction of zeolite studies, namely adsorption of adsorbates on the active site (Allavena *et al.*, 1990; Brandle and Sauer, 1997; Bredow *et al.*, 1996; Greatbanks *et al.*, 1994; Pisani and Birkenheuer, 1995; Stefanovich and Truong, 1998; Vollmer *et al.*, 1999). On the other hand, the mechanical embedding approach

(Brandle and Sauer, 1998; Hillier, 1999; Ricchiardi *et al.*, 2000; Sauer and Sierka, 2000) models the crystal framework by a molecular mechanics force field but corrects the interactions in the active site region by isolated quantum mechanical cluster calculations. In this case, the lattice effects do not polarize the quantum cluster wave function but affect it indirectly via the force field. The accuracy of this approach significantly depends on the quality of potential force field, whose parameters largely depend on the set of systems and properties used in the fitting procedure. Sauer and his groups proposed a method called QM/Pot that provides good results for zeolite and related systems (Brandle and Sauer, 1997; Brandle *et al.*, 1998).

Another approach, named our Own N-layer Integrated molecular Orbital - molecular Mechanics (ONIOM) embedding procedure (Dapprich *et al.*, 1999), is different from other embedding methods. It is suitable for use with all elements without further parametrization. This idea reveals a departure from the philosophy behind methods such as QM/Pot, which employ reactive force fields finely tuned for specific systems, instead it allows a partitioning system into more than two layers and provides molecular mechanics, semi-empirical and ab initio methods for each level of theory. It is believed to be a versatile combination for modeling zeolites (Damin *et al.*, 2002a; Damin *et al.*, 2002b). The chemical information of reactions in zeolites can be obtained using smaller clusters embedded in larger clusters and using the universal force field (UFF), a generic nonreactive force field (Rappe *et al.*, 1992), as the low level of theory.

Interaction of adsorbed molecules with extra-framework cations in cation-exchanged zeolites is a key factor controlling catalytic chemical processes (Dartt and Davis, 1994; Venuto, 1994). Electrostatic fields created by these cations and surrounding framework anions contribute to polarization of adsorbed molecules, which thus find their electron distribution significantly modified. Precise characterization of the physicochemical processes occurring upon the interaction of zeolites with guest molecules is a prime requirement to understand chemical reactivity. Complete understanding of the interaction between CO and zeolites is also of considerable interest in regard to zeolite characterization, since carbon monoxide is

the most widely used probe molecule for IR spectroscopic studies of metal oxides (Scarano *et al.*, 1998) and zeolites (Bordiga *et al.*, 1994; Lercher *et al.*, 1996; Zecchina and Otero Arean, 1996).

Low-temperature IR spectra of CO adsorbed on alkalimetal-exchanged zeolites show a main absorption band upward shifted with respect to the 2143 cm^{-1} value for free CO. The magnitude of the shift depends on the alkali metal cation and on the number of surrounding framework anions. Thus, for the series of M^+-ZSM-5 zeolites (M = Li, Na, K, Rb, Cs) this cation-specific high-frequency band was observed at wave numbers which decrease from 2188 cm^{-1} for Li^+, and 2178 cm^{-1} for Na^+, down to 2157 cm^{-1} for Cs^+ (Zecchina *et al.*, 1994), while for Na^+-Y the corresponding band shows a maximum at about 2172 cm^{-1} (Bordiga *et al.*, 1993; Knozinger and Huber, 1998). Both, experimental results and theoretical calculations show that this band corresponds to the fundamental C–O stretching mode of carbon monoxide perturbed by the electrostatic field created by cations (and surrounding framework anions) in $M^{+\cdots}CO$ adducts (Ferrari *et al.*, 1997; Ferrari *et al.*, 1996; Lamberti *et al.*, 1995).

When introduced into a zeolite matrix, transition metal ions show high catalytic activity and selectivity, while in the gas phase the same ions are either not active or too active and undergo different reactions. For example, Fe-exchanged zeolites are selective catalysts in arene oxygenation with N_2O and the active species having been identified as FeO_2^+ (Ryder *et al.*, 2003). In contrast, in the gas-phase, FeO_2^+ and benzene do not yield phenol, but undergo ligand exchange and charge exchange. The Cu-exchanged zeolites, Cu/MFI in particular, which shows high catalytic activity in direct NO_x decomposition (Giamello *et al.*, 1992; Iwamoto *et al.*, 1986), while naked Cu^+ ions do not catalyze this reaction (Koszinowski *et al.*, 2002). Cu^+ complexes with organic $[HB(tBu\text{-}pz)_3]^-$ and $[HB(Me_2\text{-}pz)_3]^-$ ligands (Ruggiero *et al.*, 1993; Schneider *et al.*, 1998), which have the negative charge and the σ-donor sites in common with the zeolite matrix (three N sites replace the O sites of the zeolite framework) and bind NO and disproportionation reactions have been observed. This suggests that the unusual catalytic activity of transition-metal exchanged zeolites must

be due to activation of the transition metal ion by the zeolite framework which functions as a specific ligand. Dramatic changes in Cu-ligand interaction upon insertion into a zeolite were clearly demonstrated for NO_2 interaction with the Cu/MFI system (Rodriguez-Santiago *et al.*, 1998).

Supported silver ions show good catalytic properties for several reactions, such as ethanol oxidation to acetaldehyde (Lai *et al.*, 1994) and aromatization of alkanes, alkenes, and methanol (Ono *et al.*, 1994). The use of silver-containing catalysts in different DeNOx processes, such as photocatalytic decomposition of NO (Matsuoka *et al.*, 1996) and selective catalytic reduction of NO_x by hydrocarbon is very promising (Sato *et al.*, 1991). However, the activity and selectivity of the catalysts depend on many factors, one of the most important being the kind of the support, which usually determines the electronic and coordination state of the cation. In many cases, the existence of cations with a high electron deficiency favors the catalytic processes.

The Brønsted acid sites of the H-ZSM-5 zeolite are among the most acidic surface OH groups that are known at present (Zecchina *et al.*, 1998). This suggests a high electron deficiency of cations exchanged in ZSM-5. Accordingly, it is reported that the Cu^+ ions in Cu- ZSM-5 possess more coordinative vacancies than do Cu^+ ions supported on oxides, e.g., silica (Hadjiivanov *et al.*, 1996). As a result, only monocarbonyls are produced after CO adsorption on Cu/SiO_2, whereas $Cu^+(CO)_x$ (x=1-3) species are formed on Cu-ZSM-5. A high electron deficiency of Na^+ cations in Na-ZSM-5 (compared to other Na^+-containing systems) was reported (Bordiga *et al.*, 1992). It may be expected that Ag^+ ions in Ag-ZSM-5 would also be characterized by a high electron deficiency and could form $Ag^+(CO)_x$ species upon CO adsorption.

Nitrous oxide (NO_x) gases have been recognized as an environmental pollutant, and they have also been identified as a greenhouse gas (Thiemens and Trogler, 1991). Several studies devoted to the development of practical catalytic approaches towards the elimination of NO_x emissions have been carried out, and a relevant part of them focused on the use of copper containing catalysts (Anpo, 1997;

Dandekar and Vannice, 1999). Lately, it was found that the Ag+ ion-exchanged zeolites display much higher activity and selectivity compared to widely used Cu+ ion-exchanged ZSM-5 zeolites towards the direct photocatalytic decomposition of NO into N_2 and O_2, as well as in the selective photocatalytic reduction of NO_x (nitrogen oxides) with ammonia or with hydrocarbons in the presence of excess amounts of oxygen (Kanan *et al.*, 2000; Li and Flytzani-Stephanopoulos, 1999; Matsuoka *et al.*, 2000; Matsuoka *et al.*, 1996).

It was in 1999 that single-wall carbon nanohorns (SWNHs) were found for the first time (Iijima *et al.*, 1999). They were discovered during an investigation of the carbon nanotube in the CO laser ablation of carbon. They were reported by the founders, Iijima et al., as an alternative topology of carbonaceous materials. Since the wall of a SWNH is a single graphene sheet, the adsorption phenomena are certainly unique (Murata *et al.*, 2000; Murata *et al.*, 2002; Ohba *et al.*, 2002). Single-wall carbon nanohorns have been shown to be efficient carriers of adsorbed methane (Bekyarova *et al.*, 2003; Murata *et al.*, 2005; Murata *et al.*, 2003) and a marvelous example of its applications is in its utilization as fuel cells (Kubo, 2002; 2004; Yoshitake *et al.*, 2002) for personal electronics.

Charlier, et al. had studied the electronic structures of SWNHs in the region close to the Fermi energy by using tight-binding and ab initio calculations (Charlier and Rignanese, 2001). The authors found that the local electronic density of the charge in SWNHs is mainly localized on the unique pentagon region. They also proposed SWNHs as good candidates for nanoprobes in scanning probe microscopy. About the same time as this finding, Shenderova, et al., using tight-binding calculations of the electronic states of SWNHs (Shenderova *et al.*, 2001) reported that a pentagon in the centre of a cone is the most probable spot for emitting tunnelling electrons in the presence of an external field. The results suggested that SWNH assemblies, if practically accessible, might be used as highly localized sources of electrons for templating at the extraordinary lithographic scale.

METHODS OF CALCULATIONS

1. Density Functional Theory (DFT)

Rising up from the idea that the total energy of a system at the ground-state can be expressed as a functional of the electron density, the Density Functional Theory (DFT) is nowadays the method of choice because of its good relation between accuracy and computational cost. By taking advantage of the DFT, it could be capable of searching for energy minima and compute several molecular properties such as atomic charges, multipole moments, vibrational frequencies, and spectroscopic constants. Briefly, DFT provides a way to obtain the electron density and the ground state energy of a polyatomic system given its atomic coordinates.

1.1 The Kohn-Sham Equations

The development of DFT in the area of computational chemistry dates from the mid 1960s when Hohenberg and Kohn demonstrated that the ground-state energy of a system of interacting electrons subject to an external potential $V(r)$ is a unique functional of the electron density (Kohn and Sham, 1965), and it can be obtained by minimizing the energy functional with respect to the density, $E = E[\rho(r)]$

$$E^{DFT} = \min_{\rho(r)} E[\rho(r)] \tag{1}$$

Later, Kohn and Sham demonstrated that there is an equivalence between the electronic density of this system (our real system) and that of a model system of noninteracting electrons which are subjected to an effective potential, V_{eff}. This provided a way to solve the problem of finding the density of the many-electron interacting system, via obtaining the electron density of the noninteracting system.

This density can be expressed in terms of single electron orbitals, $\psi_i(r)$, known as Kohn–Sham (KS) orbitals,

$$\rho(r) = 2\sum_{i}^{occ.}\left|\psi_i(r)\right|^2 \tag{2}$$

where the sum extends over the occupied single-particle orbitals (here, we restrict to the most simple situation in which all orbitals are doubly occupied). Because of the relationship in Eq. 2, the energy functional can be expressed either in terms of the density (Eq. 1) or the single-electron orbitals and the nuclear positions R_N of atoms in the system,

$$E^{DFT} = \min_{\{\psi_i\}} E^{KS}\left[\{\psi_i(r)\},\{R_N\}\right] \tag{3}$$

The energy functional (Eq. 1) can be written as:

$$E^{KS} = 2\sum_{i}^{occ.}\int \psi_i^*(r)\left(-\frac{\nabla^2}{2}\right)\psi_i(r)dr + \int V(r)\rho(r)dr$$
$$+\frac{1}{2}\int\frac{\rho(r)\rho(r')}{|r-r'|}drdr' + E_{xc}\left[\rho(r)\right] \tag{4}$$

The first term on the right-hand side of this expression is the kinetic energy of the noninteracting electrons. The second term corresponds to the interaction of the electrons with the nuclear charges and $V(r)$ is the potential as a result of the nuclei. Where only valence electrons are explicitly considered in the calculation, $V(r)$ is a pseudopotential. The third term corresponds to the classical Coulomb interaction of a density distribution ρ. The fourth term, $E_{xc}\left[\rho(r)\right]$, is a functional of the density that accounts for the remaining contributions to the electron–electron interaction.

The single electron orbitals $\psi_i(r)$ of Eq. 2 and Eq. 3 can be obtained by solving the following single-particle equations known as Kohn–Sham equations (Kohn *et al.*, 1996),

$$\left(-\frac{\nabla^2}{2}+V(r)+\int dr'\frac{\rho(r)}{|r-r'|}+V_{xc}(r)\right)\psi_i(r)=\varepsilon_i\psi_i(r) \tag{5}$$

where ε_i are the eigenvalues of the matrix of Lagrange multipliers and are called the Kohn–Sham eigenvalues or Kohn–Sham orbital energies. $V_{xc}(r)$ is the exchange-correlation potential,

$$V_{xc}(r)=\frac{\delta E_{xc}\left[\delta\rho(r)\right]}{\delta\rho(r)} \tag{6}$$

1.2 Local Density Approximation

All terms in Eq. 4 can be calculated exactly, except $E_{xc}\left[\rho(r)\right]$ for which the DFT does not provide an explicit form. The theory only demonstrates that a universal expression for it exists, $E_{xc}\left[\rho(r)\right]=\int\rho(r)\varepsilon_{xc}\left[\rho(r)\right]dr$. Usually, $E_{xc}\left[\rho(r)\right]$ is taken as the exchange and correlation energy of a uniform electron gas, which is precisely known. This is the basis of the so-called local density approximation (LDA). In this approximation, it is assumed that the exchange and correlation energy of an electron at a point depends on the density at that point instead of the density at all points in the space (Ziegler, 1991). One of the main drawbacks of LDA is that van der Waals interactions, which originate from correlated motions of electrons caused by coulomb interactions between distant atoms, cannot be properly described. Therefore, special care should be taken when addressing problems in which van der Waals interactions might play a relevant role, such as stacking interactions between π-systems and the diffusion of ligands in purely hydrophobic cavities (Kriegl *et al.*, 2003).

An extension of the LDA to unrestricted cases or open-shell systems (i.e., electronic configurations in which electrons are not paired) leads to the local spin-density approximation (LSD). In this case, not only the total density ρ, but also the electron densities of the electrons with spin α and β (ρ_α and ρ_β, respectively) are employed in the formulation. For instance, the exchange-correlation energy is expressed as

$$E_{xc}^{LSD}\left[\rho_\alpha(r),\rho_\beta(r)\right]=\int\rho(r)\varepsilon_{xc}\left[\rho_\alpha(r),\rho_\beta(r)\right]dr \tag{7}$$

A useful property to describe where α and β electrons are localized in a given system (a molecule, a molecule–ligand complex, solid, etc.) is the distribution of the spin density, i.e., the difference $\rho_\alpha(r)-\rho_\beta(r)$. For a system in which all electrons are paired (e.g., a closed-shell system) the spin density is zero at all points in space. However, any system with unpaired electrons will show regions of nonvanishing spin density. The integral of the spin density over all space (i.e., $\int_r\left[\rho_\alpha(r)-\rho_\beta(r)\right]dr$) gives the total number of unpaired electrons (i.e., zero for a singlet state, one for a doublet state, two for a triplet state, etc.).

1.3 Generalized Gradient Approximation

The accuracy provided by the local (spin) density approximation is not enough for most applications in chemistry and biology. One of its main drawbacks is that bond distances and binding energies can have large errors that appear in a nonsystematic way. This represents a serious problem for the study of ligand–protein interactions.

A step forward with respect to LDA is the so-called generalized gradient approximation GGA. This approach is based on using not only the density, but also the gradient of the density in the functional expression (Becke, 1986) in order to

account for the nonhomogeneity of the true electron density. The functional can be generically written as,

$$E_{xc}^{GGA}\left[\rho_\alpha,\rho_\beta\right]=\int f(\rho_\alpha,\rho_\beta,\nabla\rho_\alpha,\nabla\rho_\beta)dr \tag{8}$$

Several forms for the explicit dependence of the integrand f on the densities and their gradients have been proposed, including semiempirical functionals that contain parameters that have been calibrated against reference values, usually using experimental data. In practice, E_{xc}^{GGA} is usually split into two terms corresponding to its exchange and correlation contributions (i.e., $E_{xc}^{GGA}=E_x^{GGA}+E_c^{GGA}$) and separate forms for each term are provided. Among the most popular GGA exchange and correlation functionals used in chemical applications are the ones denoted as BP86 (exchange part by Becke (Becke, 1986) and correlation by Perdew (Perdew, 1986), BLYP (combination of Becke exchange and correlation developed by Li, Yang and Parr (Lee *et al.*, 1988)), PBE (developed by Perdew, Burke and Ernzerhof in 1996 (Perdew, 1986)).

The use of the GGA approximation improves considerably the description of bonding (and especially hydrogen bonding) with respect to pure LDA with a very low additional computational cost. The description of weak van der Waals interactions, however, remains problematic. Most of the applications of DFT to systems of interest use the GGA approximation. In summary, DFT provides a framework to find the total energy of a many electron interacting system by means of solving the one-electron equations of a model noninteracting system that shares the same density. Based on the generalized gradient corrections approximation and choosing a suitable exchange correlation potential, many problems of chemistry, physics, and biology can be addressed.

1.4 Hybrid Functionals

Hybrid functionals, which includes to some extent exact exchange energy in the functional expression, are also widely used. From the Hamiltonian equation and the definition of the exchange-correlation energy, an exact connection can be made between the E_{xc} and the corresponding potential connecting the non-interacting reference and the actual system. One of the most popular is B3LYP (exact exchange developed by Becke (Becke, 1993), combined with the LYP correlation functional). The exchange-correlation energy has the form of

$$E_{xc}^{B3LYP} = AE_X^{Slater} + (1-A)E_X^{HF} + B\Delta E_X^{Beck} + (1-C)E_C^{VWN} + CE_C^{LYP} \qquad (9)$$

where the exchange includes the Slater exchange E_X^{Slater}, or local spin density exchange, along with corrections involving the gradient of the density and the correlation is provided by the LYP (Lee *et al.*, 1988) and VWN by Vosko, Wilk and Nusair (Vosko *et al.*, 1980) correlations. The constants A=0.80, B=0.72, and C=0.81 are determined by Becke by fitting to the G1 molecule set (Becke, 1993).

2. Embedded Cluster Methodologies

Physical and chemical processes perceptive in biopolymers, crystals, and solutions and at their interfaces are of great importance for further progress in medicine, technology, and environmental research. Finite quantum cluster works fairly well for studying gas phase systems. It has also been used to study a specific portion of a large system while the quantum mechanical (QM) effect on the environmental region is abandoned. One possible solution of the problem is to limit the QM treatment to the active part of the system, where high accuracy is required, and to describe its environments by a less accurate method such as the semi-empirical method or simple parameterized interatomic potential function. The alternation is to use a more sophisticated method. A solution to overcome the computational limitation of expensive methods in studying extended systems is to use the fundamental idea of

the embedded cluster methodology in which the physical system is divided into two regions, the active and environmental regions. In such methods the active region consisting of atoms that are most critical to the chemistry of the system, namely the active site and adsorbate, is treated quantum mechanically at a highly accurate electron correlation level.

Generally the QM/MM approach (Hillier, 1999; Sauer and Sierka, 2000; Sherwood, 2000; Svensson *et al.*, 1996) divides the energy of the whole system S, into the energy of the active or inner part I, the potential function energy of the outer part O and an interaction term I-O,

$$E_{total}(S) = E_{QM}(I) + E_{pot}(O) + E(I-O) \tag{10}$$

The interaction term is given either by the potential function or parts of it, the electrostatic interaction and sometimes the polarization of I by O, described by the QM method. In the latter case the potential due to point charges of the outer part is simply added to the core part of the Hamiltonian.

Complication arises whenever the definition of the QM part requires cutting bonds that the link atoms need to terminate the bond, completing the valency. In the presence of link atom L we get

$$E_{total}(S) = E_{QM}(C) + E_{pot}(S) - E_{pot}(C) + \Delta \tag{11}$$

where

$$\Delta = -E_{QM}(L) - E_{QM}(L-I) + E_{pot}(L) + E_{pot}(L-I) \tag{12}$$

Term Δ will approach zero if the interatomic potential function mimics the QM potential energy surface for the terminating atoms and their interaction with the inner part (L-I). By increasing the size of the QM cluster, the interaction between the active site and the link atom region will decrease and the change of Δ will approach zero.

For relative energies, not the absolute values of Δ, but rather their change between products and reactants is important. Based on the idea of the QM/MM approach, it is not limited to use only the potential field to approximate the environmental effect in Eq. 12, it also allows the coupling of the two quantum mechanical methods when the potential function is replaced by another less expensive quantum calculation.

As an alternative, to incorporate the environmental effects of the remaining framework, two general embedding schemes have been proposed: "Electronic" and "Mechanical" embedded cluster models. In the electronic embedding calculation all terms regarded as the lattice effects are included in the Fock operator, thus the wave functions are disturbed directly via the Fock operator. On the other hand, the mechanical embedding approximates the lattice perturbation via the total energy. The most rigorous treatment of the electronic embedding scheme includes quantum mechanical effects, electrostatic Coulombic and exchange contributions between the cluster and the crystal environment. However, most of electronic embedding schemes focus only on including the electrostatic interactions of the remaining structure in the Fock matrix of a quantum mechanical cluster or embedding the cluster in the external classical electrostatic potential.

The effects of the environment on electrons in the cluster are represented by an embedding potential. The embedding potential can be generated by many different approaches. In Linear Combination of Atomic Orbital (LCAO) based method, one needs analytical expressions for the matrix elements $\langle \mu | V_{embd}(r) | \nu \rangle$ calculated over the basis functions in the cluster. For many crystals of practical interest the electrostatic, or the Madelung, potential $V_{el}(r)$ makes a dominant contribution to the total embedding potential. Adding the Madelung potential of a periodic lattice to the calculation is not a trivial task. Perhaps the best known method do this is the Ewald summation method.

The Ewald summation method is a well known technique for calculating the long-range electrostatics. This can be done by separating the potential energy, a single

slowly and conditionally convergent series, into the sum of two rapidly converging series plus a constant term. The total electrostatic interaction is calculated as

$$E^{total} = E^{real} + E^{riciprocal} - E^{correction} \tag{13}$$

where E^{real} is the screened interaction and $E^{riciprocal}$ is due to the canceling Gaussian charge distribution and $E^{correction}$ is the correction term. Although this technique provides an accurate solution for the electrostatic embedding potential, its implementation in existing molecular quantum chemistry programs requires significant efforts.

By using the concept of Conductor in an Electrostatic field as the mathematical model, a Surface Charge Representative of Electrostatic Embedding Potential or SCREEP methodology for accurately representing the Madelung potential in ab initio calculations has been proposed. This method is based on a theory from electrostatics stating that for a conductor in the electrostatic field, *i.e.*, at equilibrium, the electrostatic potential is zero everywhere inside the conductor (Stefanovich and Truong, 1998). This appears to happen because free electrons, responding to the external disturbance, readjust themselves on the surface to counterbalance the external potential. This can be shown by the equation:

$$V_{ext}(r) + \int_S \frac{\sigma(r')}{|r - r'|} dr^2 = 0 \tag{14}$$

where $V_{ext}(r)$ is the electrostatic potential due to the electron density ρ(r') outside surface S and $\sigma(r')$ is the charge density on the surface. This ensures that the mapping between charge density, no matter how complicated it is, and charge distribution over a closed surface that provides exactly the same electrostatic potential exists. For an imaginary closed surface *S* surrounding the quantum cluster, the electrostatic potential inside surface *S* due to the charge distribution outside the surface can be rigorously replaced with some surface charge density located on the surface;

$$V_{ext}(r) = -\int_S \frac{\sigma(r')}{|r-r'|} dr^2 = \int_S \frac{\sigma_s(r')}{|r-r'|} dr^2 \qquad (15)$$

where $\sigma_S(r') = -\sigma(r')$. This equation is exact for all points r on the surface S and in its interior. So, this method employs the conductor boundary conditions as a mathematical device to replace the Ewald summation of matrix elements in the quantum calculation.

In order to reduce the computational effort, the boundary element method is employed to discretize the surface S and represent ρ as a set of point charges q that satisfy the matrix equation. In this approach the surface S is divided into M surface elements with each areas S_j and the surface charge density is now represented by a set of M point charges q_j located at the centers of surface elements r_j where

$$q_j \approx \sigma_S(r_j) S_j \qquad (16)$$

Then Eq. (13) can be approximated by a matrix equation;

$$\mathbf{V} - \mathbf{Aq} = 0 \qquad (17)$$

from which the column vector of surface charges **q** can be determined by solving systems of linear equations. **V** is a column vector of the external potential at point j and **A** is the nonsingular square matrix N×N with matrix elements

$$A_{ij} = \frac{1}{|r_j - r_i|} \quad for \quad i \neq j \; and \; A_{jj} = 1.07\sqrt{4\pi / S_j} \qquad (18)$$

Nonsingular elements A_{ij} represent a generic Coulombic interaction between the surface elements r_i and r_j. The diagonal elements A_{jj} describe the self-interaction of the surface element r_j to itself (Klamt and Schuurmann, 1993). $|r_i\text{-}r_j|$ is the distance between the point charges at the positions i and j on the surface S where the potential is to be calculated. The Madelung potentials V_j are calculated by using the Ewald summation technique. The matrix inversion algorithm has been used to solve Eq. (16).

SCREEP charge q should be determined once prior to their use in embedded cluster calculations. Then, construct and discretize the SCREEP surface around a cluster.

In the SCREEP embedding approach, the embedded cluster is composed of three layers (Figure 4). At the center of the model is a quantum mechanical cluster taken from the crystal structure to represent the most important part of the system of interest. The other two layers in this model are to describe the electrostatic Madelung potential of the extended framework. The second layer is a set of partial atomic charges located at the zeolite atomic sites. This layer attempts to represent the local electrostatic interactions around the site of interest. Due to the poor convergence properties of the Madelung potential, the explicit point charges in the second layer alone are not able to accurately reproduce the electrostatic potential from the periodic framework. Another set of surface charges, determined by the SCREEP method, is added as the third layer to represent the remainder of the Madelung potential.

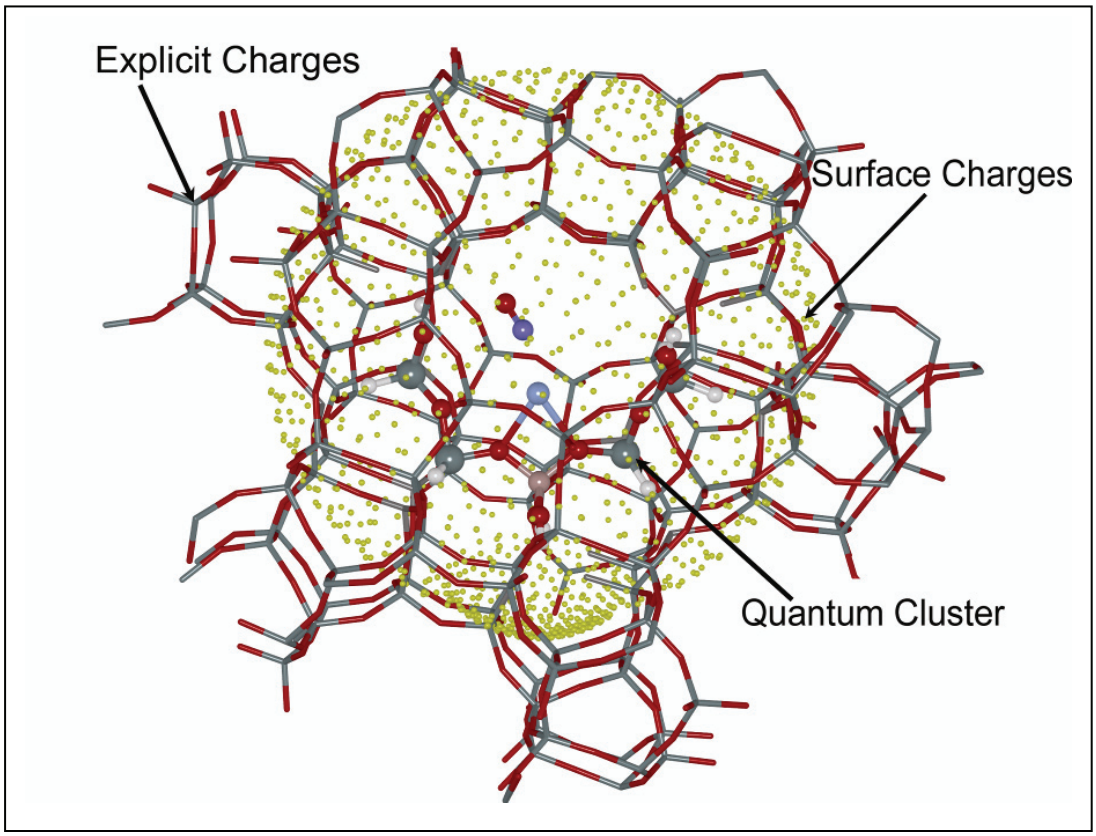

Figure 4 The embedded cluster model established from the SCREEP approach composing of 3 layers: The quantum cluster model, explicit charges and surface charges

Normally the charges are derived from a Mulliken population analysis of a periodic HF/STO-3G calculation to generate these reference potentials. However, they are very close to half of their formal charges. In this work only half of the formal charge is used. Lattice charges closed to the cluster are treated explicitly and thus the electrostatic potential resulting from these charges are exact. Electrostatic potential from the rest of lattice point charges, not included as explicit charges, is recovered by the potential from the surface charge. This separation can dramatically decrease the error resulting from discretizing surface charge density to point charges on the surface. The shape of surface S is arbitrary.

Due to the partial covalent nature of zeolites, hydrogen link atoms are used to terminate the cluster's dangling bonds to saturate the atomic valency of the cluster atoms at the border, but special care has to be taken. A practical and widespread solution is the use of hydrogen atoms to terminate the dangling bonds of the active part. The terminating H atoms play the role of a quarter of a silicon atom or of a one half of an oxygen atom. The electronegativity of H is between that of Si and O; H accepts electrons from Si (as O does), and it donates electron density to O (as Si does). The difficulty in this region is the strong interaction between the explicit point charges and the artificial saturating hydrogen atoms of the cluster. This interaction is particularly strong with the first shell of explicit point charges (the set of point charges nearest to the quantum cluster) since they are often less than one angstrom away from these hydrogen atoms. It is proposed that a scheme to minimize the boundary effects would be by removing the first shell of explicit point charges and adjusting the value of the second shell of explicit point charges such that when combined with the charges of the artificial hydrogens, the Madelung potential at points inside the surface charges are reproduced.

In electronic embedding method, the boundary atoms and terminating hydrogen atoms are normally fixed at the observed atomic positions of the crystal lattice, determined either by experiments or calculations, to mimic the crystal constraint. Frequently, these positions are not accurately known or are known only as an average structure of analogous crystals that do not reflect the active site properties.

Adopting such atomic positions introduces artificial strain which could be minimized when a theoretically predicted structure is used. The active region, the most interesting part and the part which is mainly disturbed by the adsorbate, is allowed to relax.

3. Details of Calculations

Zeolite catalysis is of prime importance in many industrial processes due to the size- and shape-selectivity of zeolite crystals and their Brønsted acid sites (Blaszkowski and van Santen, 1995; Chu and Chang, 1985; Das *et al.*, 1992; Hass and Schneider, 1996; Kassab *et al.*, 1993; Klinowski, 1991; Kramer *et al.*, 1993; Krossner and Sauer, 1996; Makarova *et al.*, 1995; Soscun *et al.*, 1995). Recently, metal-substituted zeolites were found to be potential catalysts for decomposition of NO_x and CO from automotive emission and power plants (Bell, 1997; Katoh *et al.*, 1995). CO adsorption is also used as a probe of the cation loading in ion-exchange processes in zeolites (Katoh *et al.*, 1995). For this reason, numerous theoretical and experimental studies have been performed to examine the interaction of CO with zeolites (Bates and Dwyer, 1993; Dixon *et al.*, 1988; Ferrari *et al.*, 1996; Hass and Schneider, 1996; Ikuta, 1984; 1985; Neyman *et al.*, 1995; Sauer *et al.*, 1994; Schneider *et al.*, 1996; Senchenya *et al.*, 1996; Trout *et al.*, 1996; Ugliengo *et al.*, 1989; Zhanpeisov *et al.*, 1996). To the best of my knowledge, theoretical studies to date are based on small quantum clusters as models of the zeolite Brønsted acid site. Such cluster models can sometime give reasonable estimates of adsorption energy. However, the model does not correspond to any specific zeolite, but rather to a generic tetrahedral subunit containing the Brønsted acid site in an unconstrained environment. Recent studies have shown that the Madelung potential is important in studying adsorption processes due to its long-range electrostatic nature (Greatbanks *et al.*, 1994; Stefanovich and Truong, 1998).

To include the effects of the zeolite framework on the adsorption of CO in zeolites, a periodic electronic structure method can be utilized (Campana *et al.*, 1994; Teunissen *et al.*, 1994b). This corresponds to the high loading case and is often

computationally expensive for most zeolites due to their relatively large unit cells. Alternatively, the embedded cluster approach provides a more practical methodology with little additional computational cost as compared to the bare cluster calculations (Stefanovich and Truong, 1998).

3.1 Adsorption of CO in H-ZSM-5 and Li-ZSM-5 zeolites

In this study, I examined the interaction of CO in both H-ZSM-5 and Li-ZSM-5 zeolites. Particularly, I focused attention on the importance of the Madelung potential in the structure and energetics of CO adsorption in these zeolites. Cluster and embedded cluster models were used to determine the structure and energetics of species in H-ZSM-5 and Li-ZSM-5 zeolites. The quantum cluster in both models consists of three tetrahedral sites including the Brønsted site with capped hydrogen atoms at the boundary, i.e., $H_3SiO(X)Al(OH)_2OSiH_3$ called 3T model where X is either a H or Li atom. The Si–H bonds are fixed along the Si–O bonds of the ZSM-5 framework (Klinowski, 1991).

In embedded cluster models, the total Madelung potential of the ZSM-5 zeolite framework is represented by 201 explicit charges within 3.5 Å to the quantum cluster and 688 surface charges. For comparison between the reactivity of active site in different types of zeolites, the total Madelung potential of the FAU zeolite framework is represented by 1137 explicit charges within 3.5 Å to the quantum cluster and 146 surface charges. With this small number of point charges, additional computational cost is often less than 5% compared to bare cluster calculations.

Geometry optimizations were done at the HF level using the 6–31G(d,p) basis set. Capped hydrogen atoms were fixed along the Si–O bond during these optimizations. For CO adsorption on H-ZSM5 and Li-ZSM5, two possible adsorption configurations were investigated. One is called C-bound where CO approaches the zeolite with the C-end. Similarly, the O-bound complex means the O-end approaching the zeolite. Geometries of these complexes are fully optimized without additional constraints besides those of the capped hydrogen atoms.

3.2 Adsorption of NO and CO on Ag-ZSM-5

Transition metal exchanged zeolites have been the focus of experimentalists for decades due to their catalytic properties over other transition metal or oxide catalysts in many reactions, such as NO_x decomposition. Oxides of nitrogen in the atmosphere, which are a major target of clean air policies, can be decomposed into non-toxic gases over transition metal catalysts or by selected catalytic reduction processes. Iwamoto and his co-workers (1986) suggested a simpler and cleaner way by using metal exchanged zeolite as a catalyst for the direct decomposition of NO into N_2 and O_2. Cu exchanged zeolites have been reported as catalysts for the decomposition of NO at high temperature since the late 1970's. Subsequently, Ag exchanged zeolites were found to be more reactive. The comparison between Cu-ZSM-5 and Ag-ZSM-5 has been the focus of some experimental studies. Despite the abundance of studies, the knowledge about such reactions is still far from being fully understood. Theoretical study is an alternative way to compliment the information about such catalysts and their chemistry. Chen and Yang used HF and MP2 methods to study the adsorption of O_2, N_2 and ethylene on Ag-ZSM-5 and they used orbital population analysis to explain interactions between zeolite and adsorbates (Chen and Yang, 1996). Kanougi and co-workers used molecular dynamic calculations and local density functional theory to study the coordination of exchanged metals, i.e., Ga, In, Cu, Ag and Co, in the ZSM-5 framework and predicted that these ions bind to two framework oxygen atoms (Kanougi *et al.*, 1997). Nachtigall and co-workers applied the QM-Pot method to study the stability of Ag^+ ion sites in Ag-ZSM-5, and also its excited state regarding the photocatalytic property in the NO decomposition process (Nachtigall and Nachtigallova, 2000). Those studies provide insight into the Ag-ZSM-5 system in such respects as coordination, stability and adsorption modes. However, knowledge about Ag-ZSM-5 and its reactivity is still far from complete. To my knowledge, there is no theoretical work focusing on adsorption of NO on Ag-ZSM-5 that has previously published before.

In the present work, I am investigating the structure of the active site of the Ag-ZSM-5 zeolite and the adsorption properties of NO on this zeolite. Both cluster and embedded cluster methodologies were employed to study the effects of the cluster size and of the Madelung potential. From a theoretical point of view, I found that the effects of the cluster size and of the Madelung potential are perceptible in the Ag+ binding energy and the location in the zeolite environment.

The active site of Ag-ZSM-5 was represented by clusters of 3T and 5T (T represents Si- or Al- tetrahedral) taken from the periodic silicious ZSM-5 structure. The clusters were terminated by hydrogen atoms, along broken Si-O bonds in the zeolite lattice. An Ag^+ ion was added to the cluster to compensate a negative charge that resulted from Al substitution. The Al atom was placed at the T12 site, an intersection of the main channel and the zigzag channel of the ZSM-5 framework. This site was predicted to be one of the most energetically favorable sites for Aluminum in the zeolite framework. An exchanged Ag^+ cation binding to two bridging oxygen atoms points directly to the intersection of two channels, thus it is accessible for adsorbates and is considered as a reactive catalytic site. The effect of the Madelung potential from the remaining part of ZSM-5 crystal was included using the SCREEP embedding scheme. Briefly, the Madelung potential from the extended zeolite framework can be mimicked by a set of point charges located on the surface enveloping the cluster (Figure 4). More details on the SCREEP method can be found elsewhere. Previous studies on several systems showed the electrostatic potential from the zeolite framework can be replicated very precisely by this method.

Density Functional Theory (DFT) with B3LYP functional was used for all structural determination. The 6-31G(d,p) basis set was employed for all atoms except Ag, which was represented by the Hay-Wadt VDZ_{n+1} basis set. For all optimizations, only the geometries of the active site and adsorbate were optimized while the remaining part of the quantum cluster was fixed to the crystal structure. Since dispersion interaction may be important for adsorption of NO and CO on Ag-ZSM-5, and it is questioned if DFT can account for such interactions accurately, single-point calculations at the Møller Plesset Theory MP2 level of theory were also performed on

the B3LYP-optimized structures. Basis set superposition error (BSSE) correction as well as zero point energy (ZPE) correction were included in calculations of adsorption energies. In addition, natural bond orbital analysis (NBO) was performed (Reed *et al.*, 1988) to examine the interactions between exchanged Ag^+ ion and CO/NO probed molecules. All calculations were done using the Gaussian 98 program.

3.3 Interaction of a gold atom with carbon nanohorn and carbon nanotube tips and their complexes with a CO molecule

In order to comprehend the difference between the properties of the single-wall carbon nanohorn tip and the single-wall carbon nanotube tip, the density functional theory (DFT) method was employed. Models comprising the equivalent number of carbons to be representative of a single-wall carbon nanohorn ($C_{80}H_{20}$) and the tips of a single-wall carbon nanotube ($C_{80}H_{10}$) that are sufficiently large (cf. Figure 5). To ascertain the most favorable site for the gold atom, nine positions among the analogous region of SWNH and SWNT tips were taken into consideration. To observe the property of the gold atom on different supporting materials, a carbon monoxide molecule was used as a probe molecule for investigating and comparing the reactivity of the gold atom on the tips of both the carbon nanohorn and carbon nanotube.

All the calculations were performed at the density functional theory (DFT) with the Perdew, Burke and Ernzerhof (PBE) non-local generalised gradient functional (Perdew, 1986). The standard split-valence polarization SV(P) (double-ζ with polarization) basis sets were employed. For Au, relativistic effects were included via an effective core potential (ECP) that leaves 19 valence electrons to be treated explicitly by (7s6p5d)/[6s3p2d] contraction. All optimization processes were done using the Turbomole 5.7 code (Ahlrichs *et al.*, 1989). With the intention of reducing the computational time, the coulomb interactions were efficiently treated by resolution of the identity (RI) technique (Eichkorn *et al.*, 1995). This method has been shown to be superior to pure DFT calculations. A counter-poise (CP) correction (Boys and Bernardi, 1970) for basis set superposition error (BSSE) was applied to the

calculations of the interaction energies. The π-orbital axis vector (POAV) analysis (Bronstein *et al.*, 2002) was performed to facilitate predicting the sp^2-sp^3 hybridized alteration capability of such carbon in the system. In previous work, the POAV analysis had successfully predicted the chemical reactivity of the sidewall of the SWNT (Warakulwit *et al.*, 2005). The outputs were imported to the charge-partitioning scheme (Reed *et al.*, 1988) from natural population analysis (NPA) implemented in a Gaussian 03 package (Frisch *et al.*, 2004).

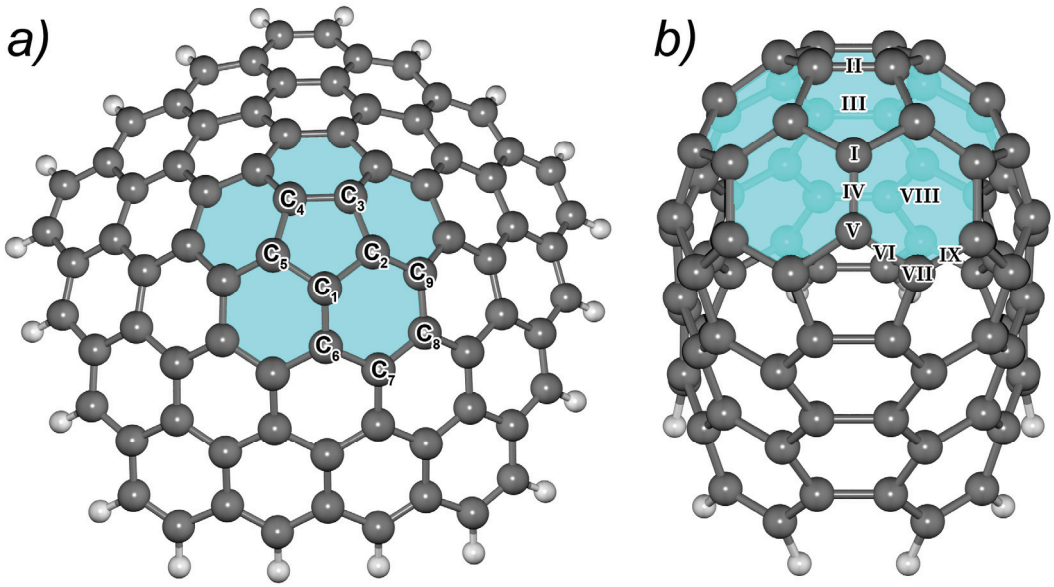

Figure 5 Cluster models for a) carbon nanohorn ($C_{80}H_{20}$) and b) carbon nanotube ($C_{80}H_{10}$) tips. Nine positions (site I-IX) among an analogous region (shaded area) of both models were examined as to whether they could be the possible sitting sites for the gold atom. Both of the tips share the same atom and site labeling.

RESULTS AND DISCUSSIONS

1. Adsorption of CO in H-ZSM-5 and Li-ZSM-5 zeolites

The structure of cluster and embedded cluster models for the HZSM-5 zeolite are carefully examined and shown in Figure 6. Selected optimized geometrical parameters and partial charges at the Brønsted site are documented in Table 1. Comparing results between cluster and embedded cluster models, the Madelung potential has an effect of elongating the O_2–H_b bond distance (Brønsted acid site) by less than 0.01 Å and increasing the positive charge on H_b atom by 0.02 AU, thus, enhancing the acidity of the Brønsted acid site. Our results are similar to those obtained by Greatbanks et al. using a different embedded cluster approach with potential derived charges. The calculated Al–H_b distance of 2.338 Å from the embedded cluster model is also consistent with the NMR measurement of 2.38±0.04 Å. As noted above, the Madelung potential was found to also lengthen the Al–H_b distance by about 0.01 Å. This is within the uncertainty of the experimental data. Thus, the Madelung field has a small effect on the structure of the Brønsted site. However, it was found to have a larger effect on the energetic properties as discussed below.

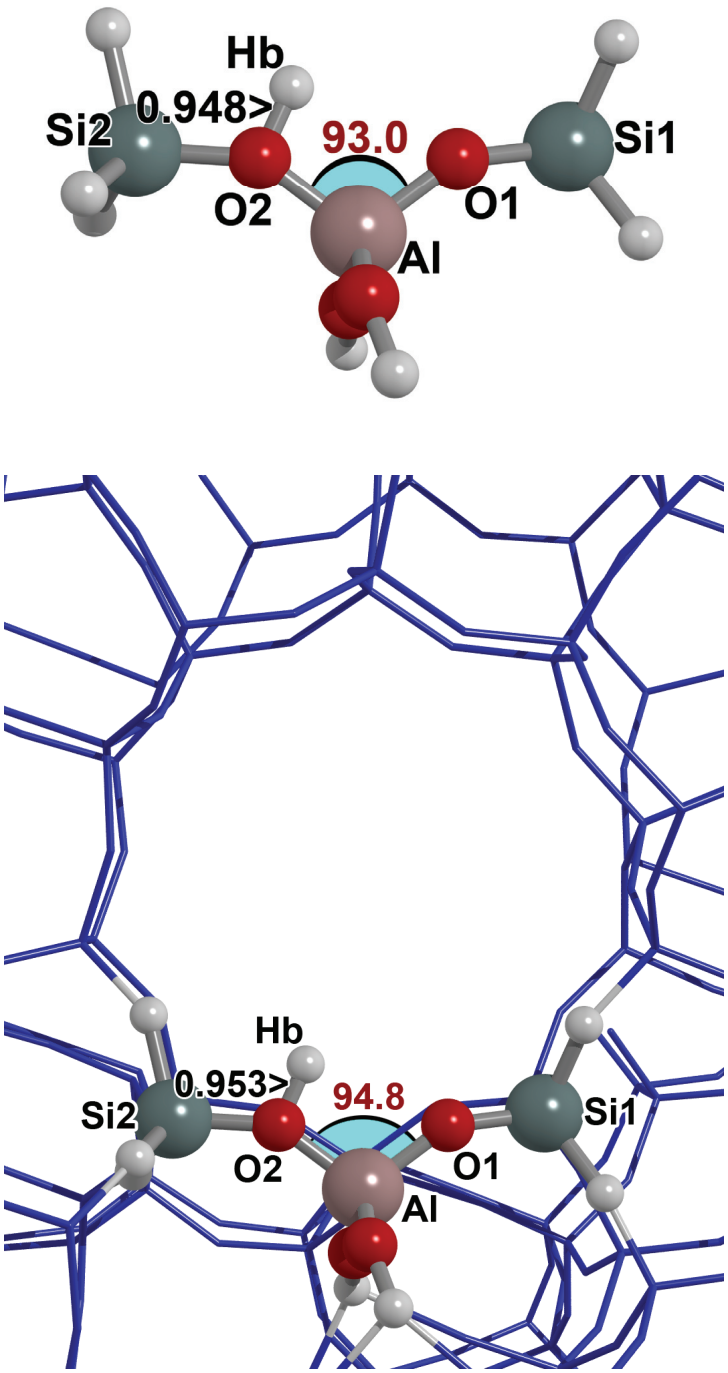

Figure 6 Cluster and embedded cluster models of the H-ZSM-5 zeolite. Bond distances given in the figures are in Å and bond angle is in degrees.

For the Li-ZSM-5 zeolite see Figure 7, the Li cation does not bind to a particular bridging oxygen atom but rather symmetrically bidentates to O_1 and O_2 atoms of the [AlO_4] tetrahedron as confirmed by an ESR experiment. Geometrical parameters of the Li-ZSM5 are listed in Table 2. The bare cluster calculations predict the Li cation to be out of the (O_2, Al, O_1) plane by 5^o in the Li–O_2–O_1–Al dihedral angle. The Madelung potential brings the cation to within 1^o in this dihedral angle from being in the same plane. However, the interaction of Li cation with zeolite leads to substantial perturbation on the zeolite framework near the active site. In particular, comparing the embedded cluster results listed in Tables 1 and 2 for H-ZSM5 and Li-ZSM-5 systems, I found the Al–O_2 distance is shorten by 0.109 Å while the other Al–O_1 distance is elongated by 0.077 Å; similarly, the Si–O_2 bond shorten by 0.068 Å while the Si–O_1 bond elongated by 0.02 Å; but the O_1–Al–O_2 angle has no significant change upon metal exchange. In a reciprocal effect, the zeolite framework reduces the Li cation charge to 0.72 AU. The Madelung potential was found to have a larger effect on the structure of Li-ZSM-5 zeolite. Particularly, it elongates the Al–Li distance by 0.54 Å and decreases the O_1–Li–O_2 angle by 2.6^o. This indicates the Madelung field weakening the attachment of the Li cation to the zeolite framework. One can expect that in this case, adsorption on the Li-ZSM-5 will be affected by the presence of the Madelung potential.

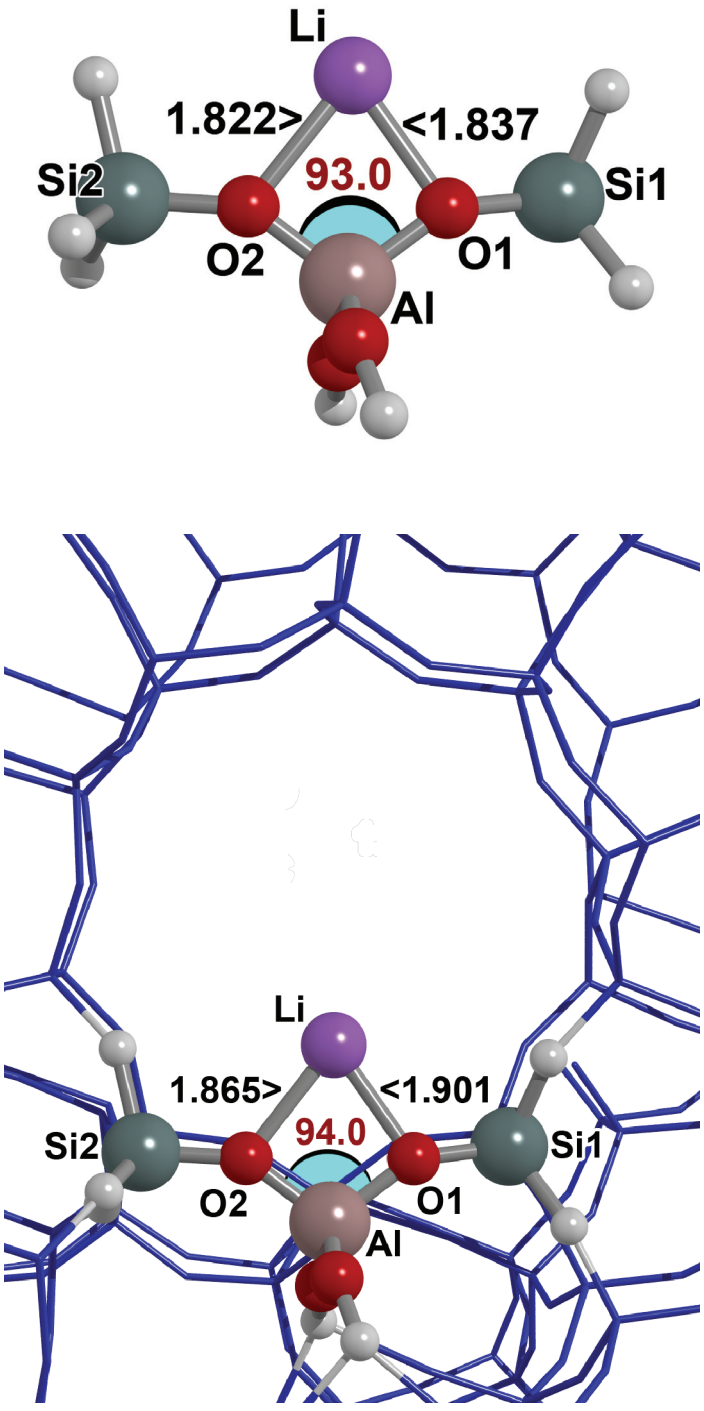

Figure 7 Cluster and embedded cluster models of the Li-ZSM-5 zeolite. Bond distances given in the figures are in Å and bond angle is in degrees.

Table 1 HF/6–31G** optimized geometrical parameters of the H-ZSM-5 and H-ZSM-5/CO systems (bond lengths are in Å and bond angles in degrees).

Parameters	H-ZSM-5		H-ZSM-5/CO			
	Bare cluster	Embedded cluster	Bare cluster		Embedded cluster	
			C-bound	O-bound	C-bound	O-bound
Al–Hb	2.326	2.338	2.343	2.337	2.352	2.342
O2–Hb	0.946	0.953	0.953	0.951	0.960	0.956
Al–O1	1.681	1.678	1.684	1.681	1.680	1.678
Al–O2	1.866	1.859	1.861	1.863	-	-
Si2–O2	1.688	1.685	1.684	1.685	1.678	1.680
Si1–O1	1.605	1.587	1.604	1.602	1.585	1.584
C–O	-	-	1.111	1.115	1.110	1.116
Hb–C	-	-	2.230	-	2.184	-
Hb–O	-	-	-	2.147	-	2.028
O1–Al–O2	93.0	94.8	93.5	93.4	95.6	95.6
Si2–O2–Al	135.2	135.2	134.9	134.9	135.3	135.4
Hb–O2–O1–Al	181.2	177.6	183.9	183.1	179.8	178.8
Si1–O1–Al–O2	161.1	160.0	160.4	160.1	158.9	158.7
Si2–O2–Al–O1	181.5	181.4	181.3	180.8	180.8	180.7
C–O2–O1–Al	-	-	186.4	-	182.5	-
O–O2–O1–Al	-	-	-	185.9	-	180.8
q(H)	0.415	0.435	0.436	0.441	0.454	0.464
q(O1)	-0.914	-0.884	-0.924	-0.912	-0.886	-0.882
q(O2)	-0.802	-0.805	-0.835	-0.824	-0.843	-0.832

Table 2 HF/6–31G** optimized geometrical parameters of the Li-ZSM-5 and Li-ZSM-5/CO systems (bond lengths are in Å and bond angles in degrees).

Parameters	Li-ZSM-5		Li-ZSM-5/CO			
	Bare cluster	Embedded cluster	Bare cluster		Embedded cluster	
			C-bound	O-bound	C-bound	O-bound
Li–Al	2.519	2.573	2.533	2.535	2.588	2.583
Li–O1	1.837	1.901	1.851	1.852	1.920	1.914
Li–O2	1.822	1.865	1.832	1.837	1.874	1.875
Al–O1	1.758	1.755	1.755	1.755	1.753	1.752
Al–O2	1.760	1.750	1.757	1.757	1.747	1.747
Si–O2	1.626	1.617	1.623	1.623	1.614	1.614
Si–O1	1.624	1.607	1.621	1.620	1.606	1.605
CO	–	–	1.107	1.118	1.109	1.117
Li–C	–	–	2.343	–	2.353	–
Li–O	–	–	–	2.078	–	2.064
O1–Li–O2	88.4	85.8	87.7	87.5	85.1	85.3
O1–Al–O2	93.0	94.0	93.2	93.2	94.3	94.3
Si–O2–Al	130.1	131.4	130.3	130.3	131.7	131.7
Li–O2–O1–Al	185.1	178.6	184.4	185.1	178.5	178.6
C–O2–O1–Al	–	–	183.1	–	183.2	–
O–O2–O1–Al	–	–	–	183.6	–	183.7
$q(Li^+)$	0.666	0.719	0.515	0.609	0.570	0.658
q(O1)	-1.011	-0.991	-1.011	-1.013	-0.991	-0.993
q(O2)	-1.011	-0.999	-1.011	-1.012	-0.998	-0.999

Cluster and embedded cluster models for the adsorption of CO on H-ZSM-5 and Li-ZSM-5 zeolites are illustrated in Figs. 7 and 8, respectively. Selected geometrical parameters of the adduct complexes are listed in Tables 1 and 2. Adsorption energies calculated by using different models are given in Table 3.

It is found that adsorption of CO does not affect the zeolite framework significantly, though this can be expected due to the small dipole of CO. The geometry of the H-ZSM-5 or Li-ZSM-5 Brønsted site changes by at most 0.01 Å for bond distances and 1^{o} for angles due to CO adsorption. This result has an important implication that is in future theoretical studies of adsorption of similar species; it is possible without loosing much accuracy to fix the zeolite framework in optimization of the complex structure. This would accelerate the convergence and reduce significantly the computational cost.

For the C-bound complex on H-ZSM-5, the distance from the C atom to the Brønsted proton was predicted to be 2.230 Å using the cluster model. Including the Madelung potential shortens this distance by 0.046 Å. The effect is noticeably smaller for adsorption on Li-ZSM-5. It is interesting to note that adsorption of CO increases the charge of the Brønsted acid proton by more than 0.02 AU, whereas it decreases the Li cation charge by as large as 0.15 AU.

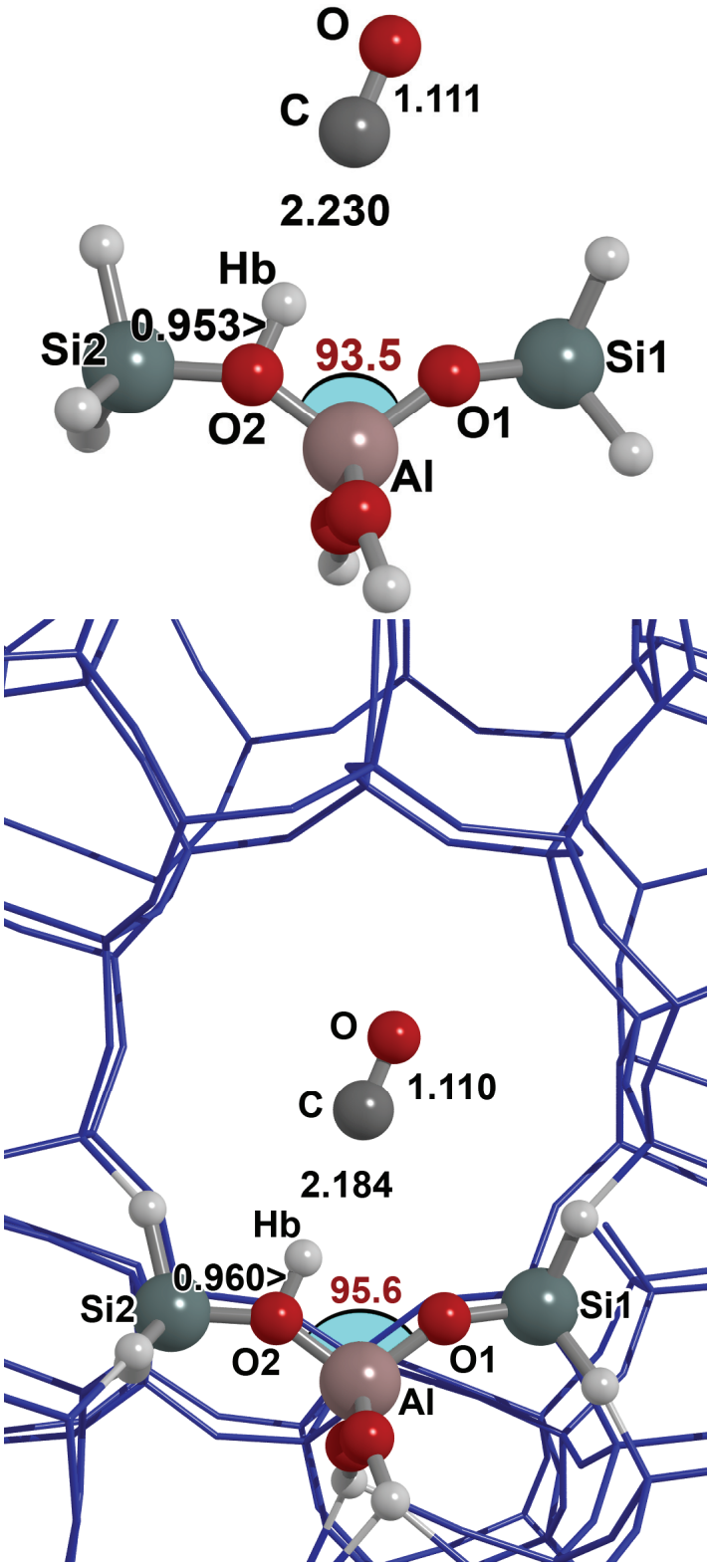

Figure 8 Cluster and embedded cluster models of the H-ZSM-5/CO complex. Bond distances are in Å and bond angle is in degrees.

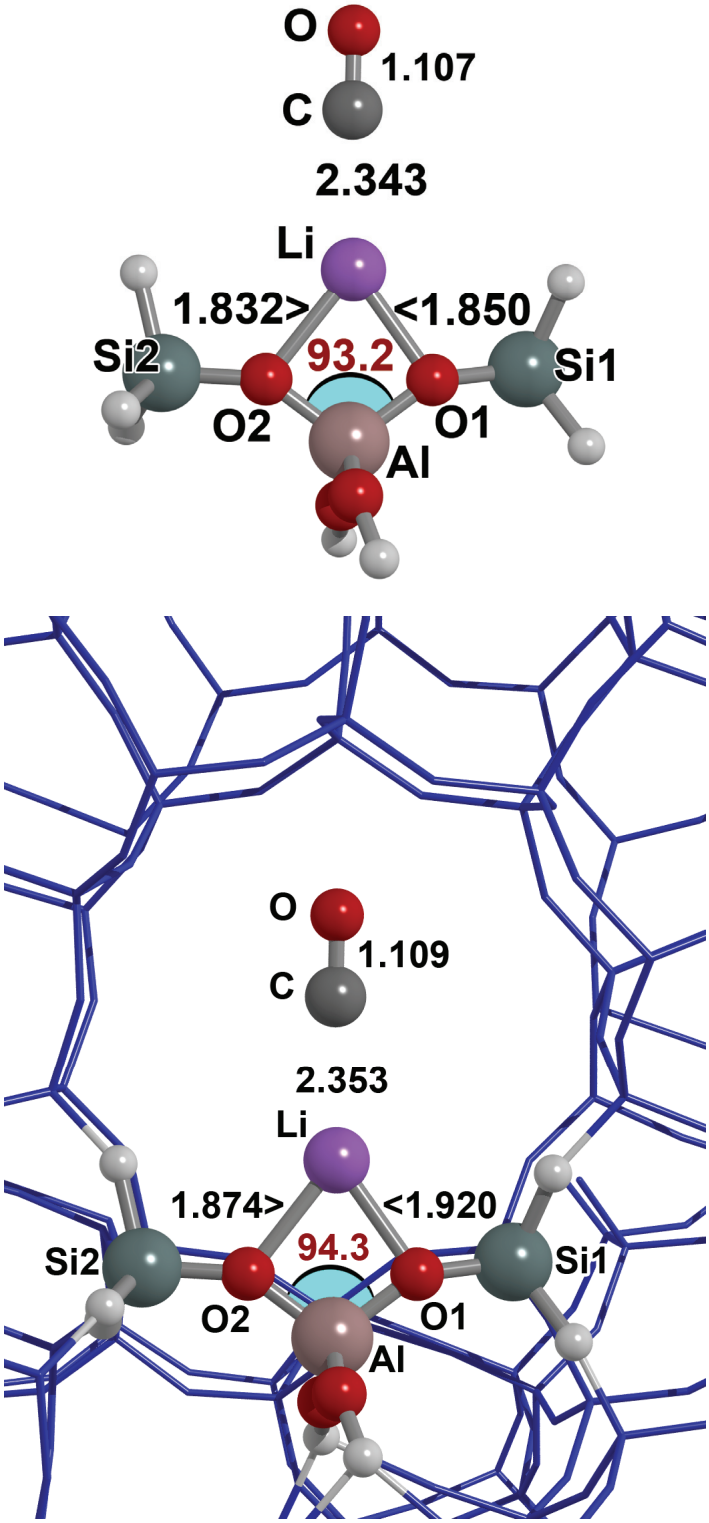

Figure 9 Cluster and embedded cluster models of the Li-ZSM-5/CO complex. Bond distances are in Å and bond angle is in degrees.

Table 3 Calculated adsorption energies (kcal/mol) of CO on naked Li(I), bare quantum cluster and embedded cluster model of H-ZSM-5 and Li-ZSM-5 zeolites.

Adsorption Energies (kcal/mol)	Bare cluster		Embedded cluster	
	C-bound	O-bound	C-bound	O-bound
ΔE: H-ZSM-5/CO	-3.61	-2.26	-6.09	-4.75
ΔE(BSSE): H-ZSM-5/CO	-2.25	-1.41	-4.95	-3.62
ΔE: Li-ZSM-5/CO	-8.04	-7.90	-10.78	-10.38
ΔE(BSSE): Li-ZSM-5/CO	-5.77	-5.56	-8.56	-8.03
ΔE: Li^+/CO	-14.62	-16.44	-	-
ΔE(BSSE): Li^+/CO	-13.14	-15.25	-	-

The effects of the Madelung potential are more profound in the adsorption energies of CO on both H-ZSM-5 and Li-ZSM-5 as listed in Table 3. For the adsorption of CO on H-ZSM-5 zeolite, it is found that both bare cluster and embedded cluster models predict both C-bound and O-bound adducts existed with the C-bound being more stable by 1 kcal/mol. For adsorption of CO on Li-ZSM-5 zeolite, C-bound and O-bound complexes have almost the same binding energy within the uncertainty of the calculations. It is noted that the Madelung potential increases the binding energy by about 2.5 kcal/mol in the H-ZSM-5 and about 3.0 kcal/mol in the Li-ZSM-5 zeolite. With inclusion of basis set superposition error (BSSE) correction calculated using the counterpoise correction method and effects of Madelung potential, CO adsorbs on H-ZSM-5 zeolite in a C-bound complex preferably with a binding energy of 4.95 kcal/mol. This is in consistent with the experimental range of 3.25–4.10 kcal/mol obtained by Gupta et al. for a lower acidic zeolite H–X using a range of acidic site compositions. For Li-ZSM-5 zeolites, both adducts exist with the C-bound configuration being slightly more stable and having the binding energy of 8.56 kcal/mol. Again this is in reasonable agreement with the binding energy of 6.7

kcal/mol for adsorption of CO on Na–Y zeolite. Since the size of Na^+ ion is larger than that of Li^+ ion, one can expect that CO would bind more strongly to Li-ZSM-5 than Na-ZSM-5. It is interesting to compare the adsorption of CO on Li-ZSM-5 zeolite with the case where the zeolite framework is absent, i.e., in the naked Li^+–CO system. The adsorption energies for both C-bound and O-bound Li^+–CO complexes are also listed in Table 3. As expected, the CO binds much more strongly to the Li^+ cation than in the Li-ZSM-5 zeolite by almost twice in the binding energy. An interesting result is that the O-bound complex is more stable by about 2.11 kcal/mol compared to the C-bound complex in the Li^+–CO system. Thus, interactions with the ZSM-5 zeolite framework reverse the order of relative stability of these complexes.

Another point of interest is the comparison of the results obtained using both cluster and embedded cluster models for exploring the different types of zeolites. The effects of the Madelung potential are more profound in the adsorption energies of CO on both H|Li-ZSM-5 and H|Li-FAU zeolites, as listed in Table 4.

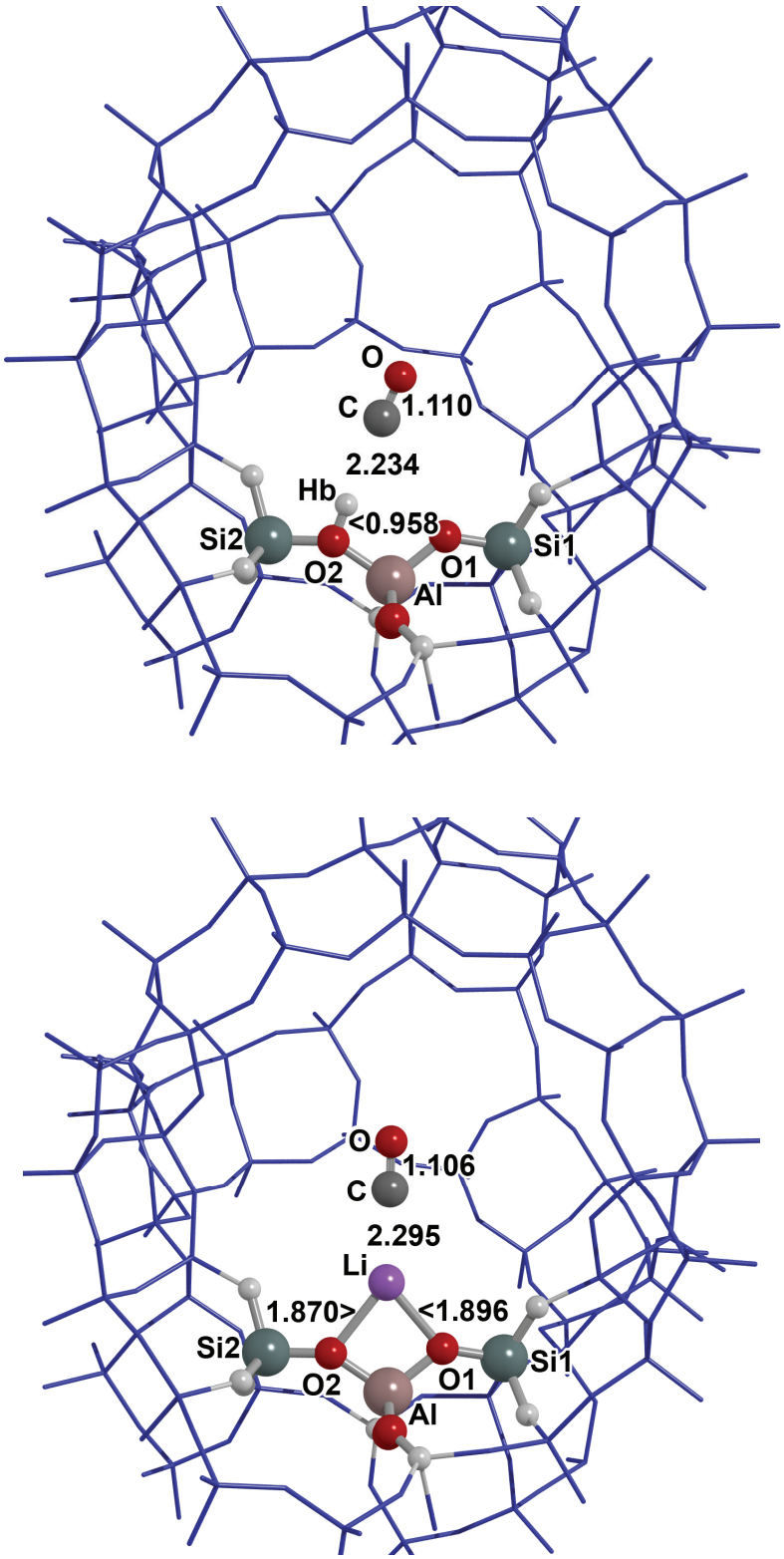

Figure 10 Cluster and embedded cluster models of the H-FAU/CO and Li-FAU/CO complex. Bond distances given in the figures are in Å.

Table 4 Calculated adsorption energies (kcal/mol) of CO on bare quantum cluster and embedded cluster model of H|Li-ZSM-5 and H|Li-FAU zeolites.

Adsorption Energies (kcal/mol)	Bare cluster		Embedded cluster	
	ZSM-5	FAU	ZSM-5	FAU
ΔE: H-Zeolite/CO	-3.61	-3.18	-6.09	-4.34
ΔE(BSSE): H-Zeolite/CO	-2.25	-1.90	-4.95	-3.20
ΔE: Li-Zeolite/CO	-8.04	-8.05	-10.78	-9.14
ΔE(BSSE): Li-Zeolite/CO	-5.77	-5.81	-8.56	-6.69

For cluster model, it is clearly seen that Li-ZSM-5/CO and Li-FAU/CO complexes have virtually the same binding energies (Table 4). It is noted that the Madelung potential increases the binding energy by 2.74 kcal/mol in the Li-ZSM-5 and by about 1 kcal/mol in the Li-FAU zeolites. With the inclusion of basis-set-superposition-error correction and the effects of Madelung potential, it could be predicted that the Li-ZSM-5/CO complex is more stable by about 1.9 kcal/mol as compared to the Li-FAU/CO complex (-8.56 vs. -6.69 kcal/mol). Thus, the Madelung potential was found to reveal that acidity of zeolite does not depend only on the acidic site center, but also on the framework structure where the acidic site is embedded. Additionally, it could be infer that the ZSM-5 is more acidic than that of FAU zeolites and leads to a better agreement with experimental observation. The results obtained in the present study suggest that the embedded cluster approach yield a more accurate and practical model than the bare quantum cluster for exploring zeolite framework and catalytic properties.

2. Adsorption of NO and CO on Ag-ZSM-5

The optimized structures of Ag-ZSM-5 in Figure 11 shows that Ag^+ ion binds to two framework-oxygen atoms, adjacent to an aluminum atom, and is in the O_1-Al-O_2 plane. The Ag…O distance is about 2.3-2.4 Å. The increasing size of cluster and the Madelung potential have similar effects on the active site structure of Ag-ZSM-5 zeolite, namely, lengthening of the Ag…O distances and shortening of the Al-O distances by about 0.1 Å. However, the Madelung potential effect on zeolite structure is more obvious than the cluster size effect as seen from data in Table 5. Madelung potential exerted to the system by using our surface charges decreases the electron density on Ag while increasing the cluster size has an opposite effect. This suggests that a larger cluster eases electron transfer from zeolite framework to an exchanged cation. Conversely, the Madelung potential diminishes such electron transfer by increasing the Ag…O distance. Increasing the cluster size from 3T to 5T can not cover all the electrostatic potential effect generated from periodic framework. In fact, the Madelung potential converges very slowly upon the increasing of cluster size. The size of a finite cluster has to be very large to substantially cover the lattice effects.

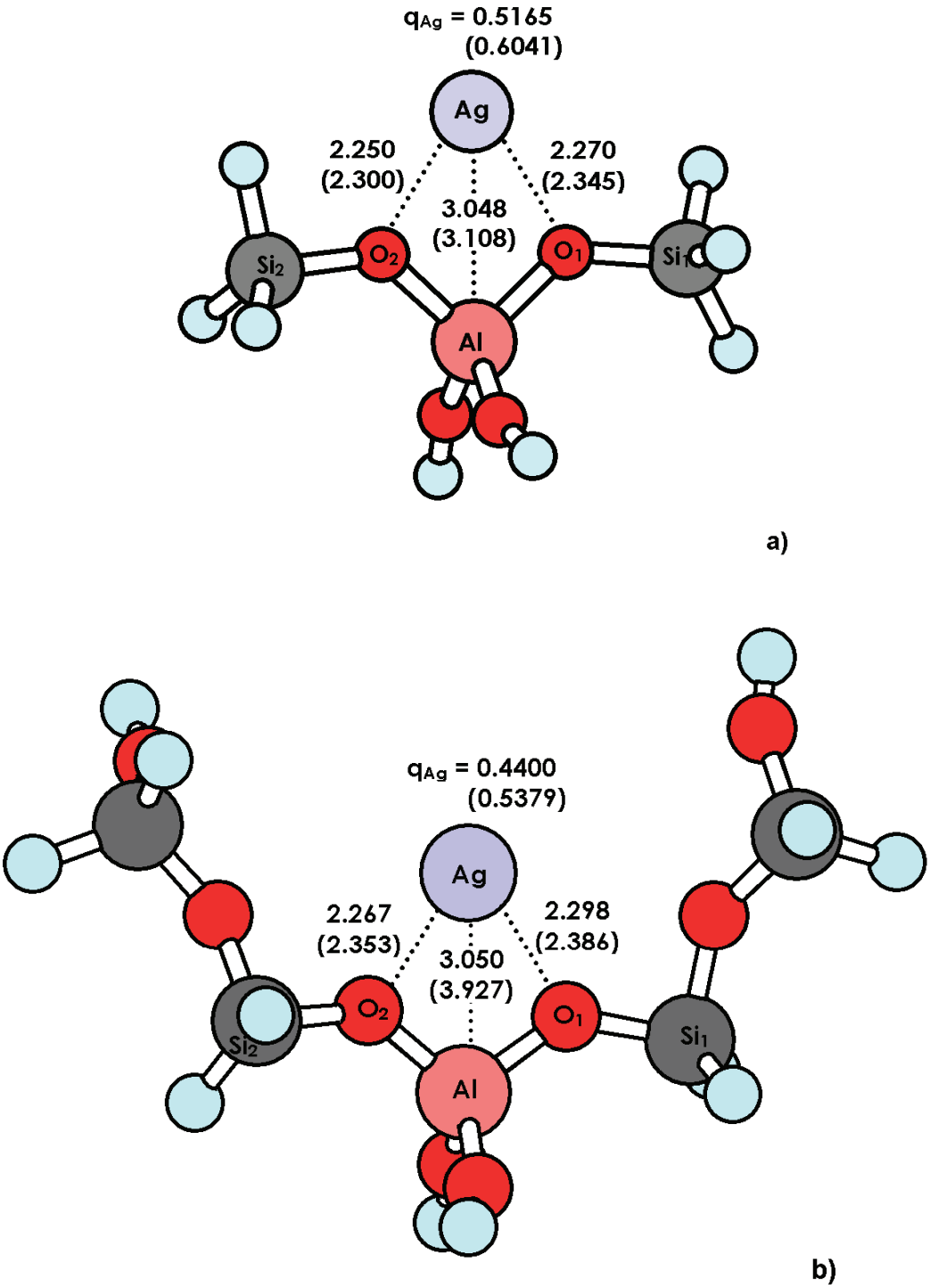

Figure 11 Ag-ZSM-5 structures optimized at B3LYP/6-31G(d,p) using finite and embedded calculation (values in parenthesis) of a) 3T cluster and b) 5T cluster; bond distance in Å.

Bordiga et.al. studied Ag-ZSM-5 zeolite by EXASF and reported that 97% of the Ag^+ ions are presented as isolated ions with an average Ag…O distance 2.3±0.03 Å and coordination number 2.5±0.5. These results were confirmed by QM-pot study (Ag…O = 2.32-2.36 Å). Another EXAFS study found a coordination number of 1.9 and Ag-O distance of 2.15 Å. Our embedded cluster yields Ag…O distance of 2.32-2.37 Å and double coordination of Ag^+ ion, in agreement with previous results. Due to the similarity in electronic structure of Cu and Ag cation, it is worth to make a comparison between Ag-ZSM-5 and Cu-ZSM-5. Previous studies and our calculations yield the similar result that Ag…O distance in Ag-ZSM-5 is about 0.3 Å longer than Cu…O distance in Cu-ZSM-5. Also the interaction between a cation and zeolite framework of Ag-ZSM-5 is smaller than that of Cu-ZSM-5. Since they are in the same group of the periodic table, the lower binding energy for the Ag^+ ion is mainly due to the drastically larger size of Ag^+ compared to Cu^+ therefore Ag^+ ion has less capability in accepting electron from the zeolite framework.

2.1 CO adsorption

There are two possible adsorption configurations of CO, namely C-down and O-down configurations. The C-down configuration was predicted to be much more stable than the O-down configuration. Therefore, only a C-down configuration will be discussed here (Figure 12). The adsorption of CO molecule slightly disturbs zeolite framework (Table 6). In all models Al-O and Si-O distances are barely changed upon the adsorption of CO (less than 0.003 Å) and these changes are negligible when a more realistic model, by either adding the Madelung potential or increasing the model size, is employed. The shortening of Ag…O distance by about 0.02 Å upon CO adsorption suggests more interaction between Ag cation and zeolite framework. The positive partial charge of adsorbed CO shows electron transfer from CO molecule to Ag^+ cation and thus an Ag^+ ion functions as a Lewis acid site. Ag…C-O angle is found to be linear in all models. As compared to an isolated CO bond length of 1.138 Å, the shortening of CO bond when adsorbed on Ag-ZSM-5 (0.003-8 Å) correlates to the blue-shift of CO stretching mode. Increasing the cluster

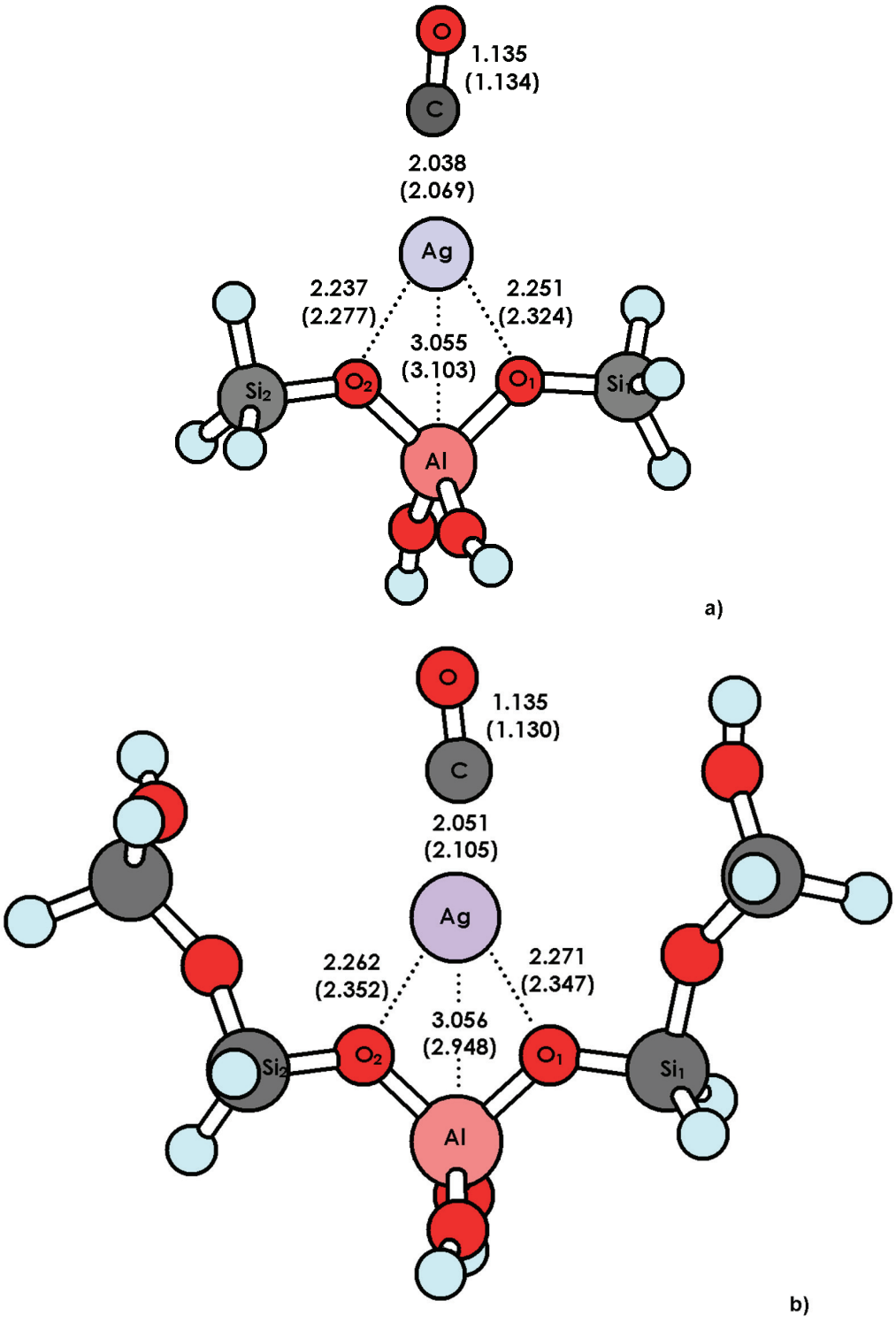

Figure 12 Optimized structures of the adsorption of CO on Ag-ZSM-5 zeolite at the B3LYP/6-31G(d,p) level using bare clusters. Selected bond distances (Å) are also given. Values in parentheses are from the embedded cluster model. a) 3T cluster and b) 5T cluster

size does not affect the CO bond length but the Madelung potential shortens the CO bond length notably by 0.005 Å. The long distance between CO and the adsorbent prohibits the direct effect of the cluster size on the CO molecule thus the long-range Madelung potential may be responsible for the changes in CO.

The binding energies of CO/Ag-ZSM-5 calculated from DFT/B3LYP for 3T bare- and embedded clusters are quite the same of about 20.2 kcal/mol. Increasing the cluster size elongates the Ag…C distance and consequently decreases the adsorption energy by about 2 kcal/mol (18.5 kcal/mol). In some systems the density functional method seems to overestimate the adsorption energy. To check this suspicion, the MP2 single point calculation on the DFT/B3LYP structure was performed. MP2 single point calculation predicted the binding energy to be 22.5 kcal/mol and 19.06 kcal/mol for embedded cluster and bare cluster, respectively. The small difference in binding energy shows that the contribution of dispersion in this system is quite small. Including the Madelung potential also elongates the Ag…C distance but it increases the adsorption energy slightly. Thus CO is stabilized in the pore by interacting not only with the active site, but also with the zeolite framework. This supports the importance of the lattice effect in the adsorption process. Comparing to our previous study, the binding energy of CO/Ag-ZSM-5 is less than 60% of the binding energy of CO/Cu-ZSM-5 (18.6 versus 33.6 kcal/mol). This may relate to a shorter cation…CO distance of CO/Cu-ZSM-5. In both cases of CO/Ag-ZSM-5 and CO/Cu-ZSM-5, linear configurations are found, agreeing with experimental prediction.

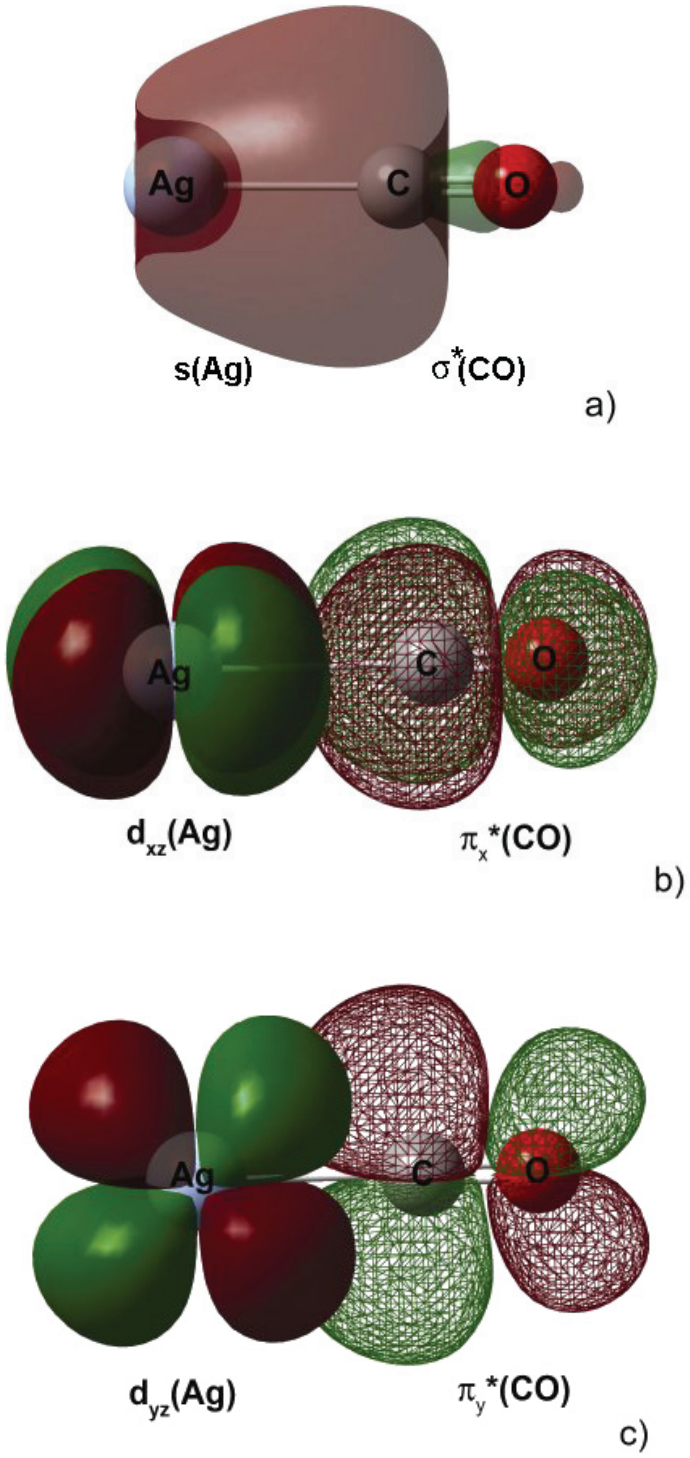

Figure 13 Natural Bond Orbital (NBO) plots showing the interaction between an exchanged Ag^+ and an absorbed CO: a) The sigma interaction between $2s^{62.73\%}2p^{37.27\%}$(C) with 5s(Ag) and the π-back bonding electron transfers between 4d(Ag) and π*(CO) b) in xz plane and c) in yz plane

To examine the electronic state of the exchanged metal, the frequency of CO stretching, which is very sensitive to its environment, was determined. The normal mode analysis predicted a blue-shift of CO stretching model upon the adsorption, corresponding to the shortened CO bond. Surprisingly, increasing the cluster size does not affect the frequency of adsorbed CO. Despite similar CO binding energy, the bare and embedded cluster models predict noticeably different CO vibrational frequencies. The Madelung effect increases the blue shifting of CO stretching by as much as 40 cm^{-1} (from 2155.4 to 2195.8 cm^{-1}), closer to the experimental range (ν=2190-2192 cm^{-1}). Our finding agrees well with the experimental observation ($\Delta\nu$=58 cm^{-1} versus 47 cm^{-1}). The interactions between CO and exchanged transition-metal zeolite can be described by σ-donating and π-back bonding. The shortening of CO bond upon the adsorption, the blue-shift of CO stretching mode and together with the NBO analysis (Figure 13) illustrate that the sigma donation from a hybrid orbital of C to s-orbital of exchanged Ag ion dominates the Ag…CO interaction. On the other hand, two π-back bondings occuring between d-orbitals of Ag^{+} and both π_x* and π_y* of CO as a consequence from the linear Ag…CO angle are quite small compared to the sigma donation.

2.2 NO adsorption

Similar to the CO adsorption, the N-down configuration of the NO adsorption on Ag-ZSM-5 was found to be more stable than the O-down configuration, thus I am focusing only on the N-down adsorption. The key difference between the CO and NO adsorption on Ag-ZSM-5 is the linear configuration for the adsorption of CO and the bend configuration ($\angle$Ag..NO $\approx$ 130º) for the adsorption of NO (see Figure 14). The bend configuration of NO/Ag-ZSM-5 contradicts to the recent MP2 result, using small cluster models, that predicted the linear form of NO adsorption on Ag-zeolite.(Zhanpeisov *et al.*, 2003) The Ag…N distance of 2.325 Å is much longer than the Ag…C distance of 2.105 Å (table 6). Furthermore, both inclusion of the

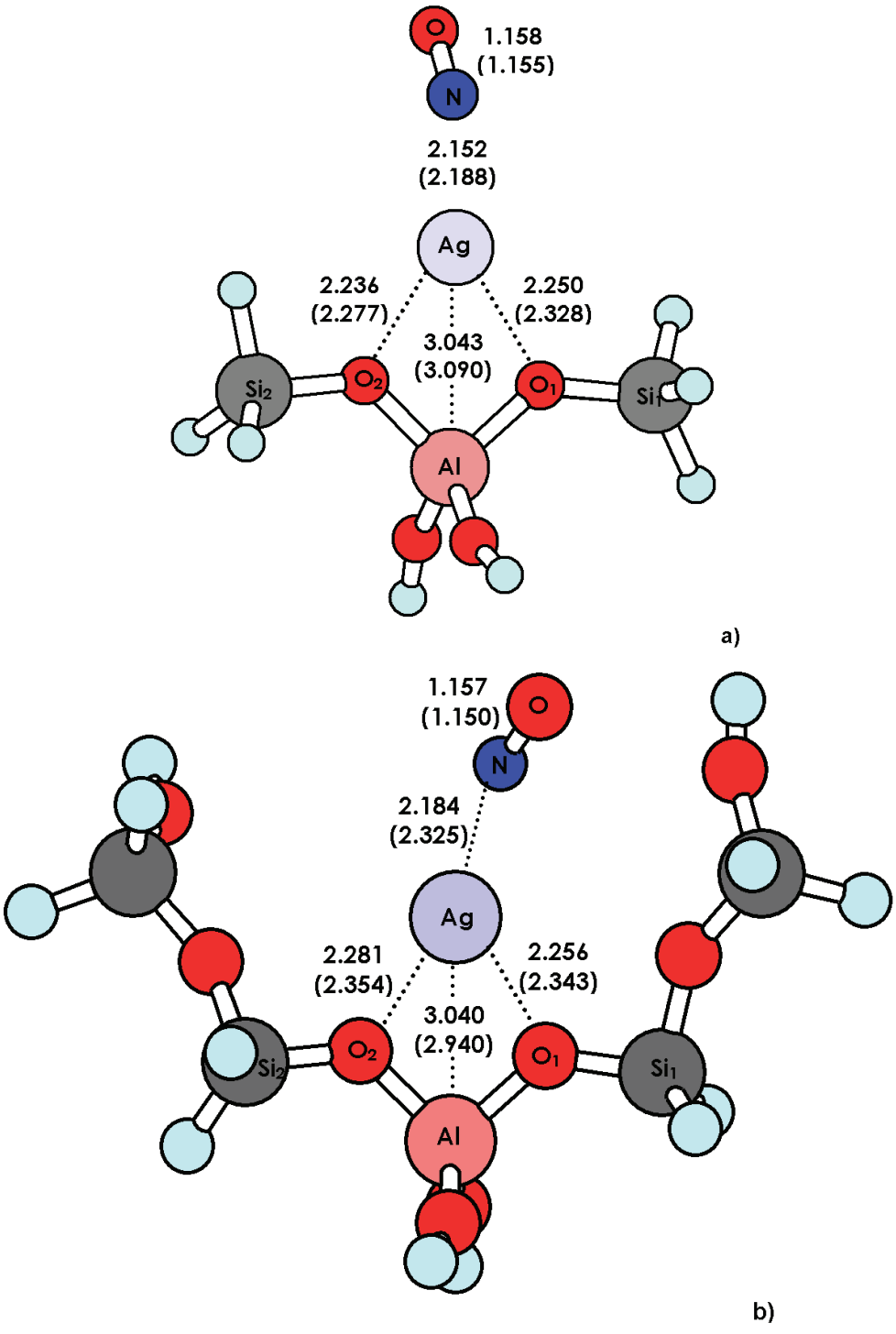

Figure 14 Optimized structures of the adsorption of NO on Ag-ZSM-5 zeolite at the B3LYP/6-31G(d,p) level using bare clusters. Selected bond distances (Å) are also given. Values in parentheses are from the embedded cluster model. a) 3T cluster and b) 5T cluster

Madelung potential and increasing the cluster size lengthen Ag…N distance. This corresponds to the decreasing in the NO binding energy. Upon adsorption, the Ag…O distance is shortened by at most 0.04 Å while the Al…O and Si…O bond lengths are almost unchanged. The adsorption of NO disturbs zeolite framework insignificantly. N-O bond is shortened by about 0.001-0.009 Å upon adsorption. This shortening is enhanced by an inclusion of the Madelung potential but is nearly unaffected by increasing the cluster size.

The bend configuration of Ag…N-O can be clearly explained by the NBO analysis as a sigma-bonding between a π* orbital (HOMO) of NO and valenced orbitals of Ag (Figure 15). The discrepancy between the recent MP2 calculation (Zhanpeisov *et al.*, 2003) and our study is probably due to the limited basis set (double-zeta without polarization and LanL2dZ) employed in the former study or the structure corresponds to the transition state converting between two symmetrically related bend structures. Since the Ag…NO distance is quite long and the orbital-overlap is limited by the bend configuration, the only occurred π-back bonding (from d-orbital of Ag ion to another π* orbital of NO) is very small compared to those found in CO/Ag-ZSM-5.

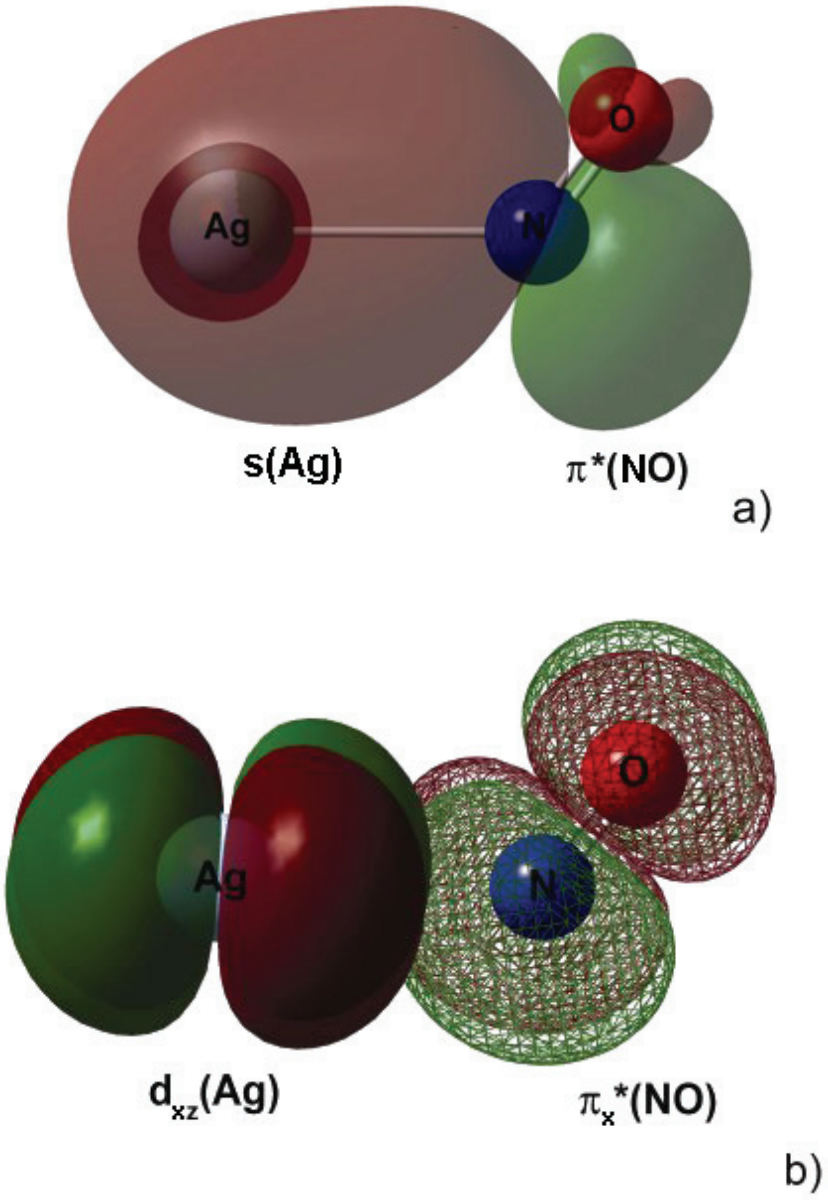

Figure 15 Natural Bond Orbital (NBO) plots showing the interaction between an exchanged Ag^{+} and an absorbed NO: a) The sigma interaction between $2s^{10.76\%}2p^{89.21\%}$(N) and 5s(Ag) b) The π-back bonding electron transfer between 4d(Ag) and π*(NO)

The binding energy of NO/Ag-ZSM-5 is predicted to be 9.24 kcal/mol by DFT/B3LYP and to be 14.14 kcal/mol by MP2 (single point calculation), much less than that of CO/Ag-ZSM-5. The difference between results from B3LYP and MP2 calculations is larger in this case. Adding the Madelung potential to the cluster lengthens Ag…N by 0.14 Å and increases the electron density on Ag center. This points out that the interaction energy between NO and Ag-ZSM-5 is not sensitive to the model of ZSM-5 but the electron density and the vibrational frequency are. Increasing the cluster size from 3T to 5T decreases the binding energy by 2.35 kcal/mol. This contrasts to the CO adsorption, in which both inclusion of the Madelung potential and increasing the cluster size increase the binding energy of CO on Ag-ZSM-5. A large difference between the NO binding energies from the 3T and 5T cluster models suggests that the 3T cluster is perhaps too small to model the active site of zeolite.

The shortening of NO bond length tentatively suggests us the blue-shift of NO stretching mode but the frequency obtained from B3LYP and MP2 calculations are slight red-shift. The stretching modes of adsorbed NO were calculated at B3LYP level from 5T bare and embedded clusters as 1828.6 cm^{-1} and 1847.2 cm^{-1}, respectively. Compared to the isolated NO (1876.0 cm^{-1}) the NO stretching calculated from our model is red-shift (-47.7 and -17.3 cm^{-1}). The red-shift of NO contradicts to experimental results which observed a slight blue-shift of adsorbed NO ($\Delta\nu$=+6 to +8 cm^{-1}). However, the inclusion of the Madelung potential shifts the frequency (up to 30 cm^{-1}) much closer to the experimental observation of slightly blue-shifted NO frequency. The sensitivity of stretching frequency of small adsorbates to its environment is well known so I presume that the calculated red-shift of adsorbed NO results from neglecting of some lattice effect beside the Madelung potential or from the harmonic potential approximation used in the frequency calculation. Nevertheless, the discrepancy in frequency shift found is quite small and irrelevant. To get the correct blue-shift matched to experimental result, a more sophisticated model including all the lattice effects and anharmonic potential approximation may be required. Recall from our previous study, NO/Cu-ZSM-5 yields a red-shift of adsorbed NO. The red-shifting of NO stretching mode in NO/Cu-

ZSM-5 is described by π-back bonding. In contrast, the long distance of Ag…NO prohibits such interaction and thus σ donating is somewhat more important in the overall reaction and results in a slight blue-shift. Our results suggest that the effects of the Madelung potential on the binding energies are small. However, it is important to obtain correct IR frequency.

The reactivity of a catalyst can be determined by its turnover rate, which is the rate of reactants undergoing reaction process per active site. This rate also depends on how easy the active site is regenerated. It was suggested previously that the reactivity of NO decomposition catalyst depends on the rate of O_2 desorption from zeolite surface to regenerate the active site. The binding energy of NO adsorbed on Ag-ZSM-5 is much less than the binding energy of NO/Cu-ZSM-5 (9.24 versus 22.80 kcal/mol). The adsorbed molecule is readily to desorb and leave the active site of Ag-ZSM-5 available for the next reactants. The substantial difference in binding energy between adsorbate/Ag-ZSM-5 and adsorbate/Cu-ZSM-5 may be an important factor for higher catalytic reactivity of Ag-ZSM-5 in NO decomposition.

Table 5 Selected parameters of Ag-ZSM5 in 3T and 5T systems (bond lengths are in Å and bond angles in degrees).

Ag-ZSM-5	3T Ag-ZSM-5		5T Ag-ZSM-5	
	Bare	**Embedded**	**Bare**	**Embedded**
O_1 – Ag	2.270	2.345	2.298	2.386
O_2 – Ag	2.250	2.300	2.267	2.353
Al – Ag	3.048	3.108	3.050	2.927
Al – O_1	1.761	1.757	1.733	1.679
Al – O_2	1.766	1.755	1.737	1.688
Si_1 – O_1	1.609	1.615	1.610	1.639
Si_2 – O_2	1.612	1.626	1.609	1.663
O_1 – Ag – O_2	69.6	67.6	68.0	67.6
O_1 – Al – O_2	94.0	94.7	94.7	103.0
Si_1 – O_1 – Al	129.7	131.2	129.6	133.8
Si_2 – O_2 – Al	129.5	130.6	131.3	132.3
Ag – O_2 – O_1 – Al	191.2	169.2	190.5	204.3
q(Ag)	0.5165	0.6041	0.4400	0.5379

Table 6 Selected geometrical parameters (bond lengths are in Å and bond angles are in degrees), Mulliken charges, frequency shifts, and binding energies for the adsorption complex of CO on the Ag-ion exchanged ZSM-5 zeolite. The frequency and binding energy data in parentheses are from single point MP2/6-31G(d,p) calculation.

CO/Ag-ZSM-5	3T Ag-ZSM-5		5T Ag-ZSM-5	
	Bare	**Embedded**	**Bare**	**Embedded**
C–O [a]	1.135	1.134	1.135	1.130
Ag – C	2.038	2.069	2.051	2.105
Ag – C – O	179.1	176.4	177.6	180.0
O_1 – Ag	2.251	2.324	2.271	2.347
O_2 – Ag	2.237	2.277	2.262	2.352
Al – O_1	1.759	1.756	1.736	1.682
Al – O_2	1.765	1.754	1.735	1.685
q(Ag)	0.4511	0.5112	0.3721	0.4233
q(CO)	0.0656	0.0908	0.0640	0.1182
$\Delta\nu_{CO}$ (cm^{-1}) [b]	+14.6	+28.1	+12.4 (+15.6)	+52.8 (+55.2)
$E_{binding}$ (kcal/mol)	20.20	20.29	18.50 (19.06)	18.63 (22.50)

[a] Isolated CO= 1.138 Å

[b] Expt: $\nu_{Isolated\ CO}$ =2143 cm^{-1} $\Delta\nu_{Adsorbed\ CO}$ = +47 to +49 cm^{-1} (Muller and Bagus, 1987; Nachtigallova *et al.*, 1999)

Table 7 Selected geometrical parameters (bond lengths are in Å and bond angles are in degrees), Mulliken charges, frequency shifts, and binding energies for the adsorption complex of NO on the Ag-ion exchanged ZSM-5 zeolite. The frequency and binding energy data in parentheses are from single point MP2/6-31G(d,p) calculation.

NO/Ag-ZSM-5	3T Ag-ZSM-5		5T Ag-ZSM-5	
	Bare	**Embedded**	**Bare**	**Embedded**
N–O [a]	1.158	1.155	1.157	1.150
Ag – N	2.152	2.188	2.184	2.325
Ag – N – O	132.0	131.5	128.1	127.5
O_1 – Ag	2.250	2.328	2.256	2.343
O_2 – Ag	2.236	2.277	2.281	2.354
Al – O_1	1.758	1.755	1.735	1.685
Al – O_2	1.764	1.753	1.735	1.685
Q(Ag)	0.4712	0.5264	0.3933	0.4287
q(NO)	0.0245	0.0650	0.0295	0.1284
$\Delta\nu_{NO}$ (cm^{-1}) [b]	-53.1	-22.0	-47.4 (-31.7)	-28.8 (-17.3)
$E_{binding}$ (kcal/mol)	11.56	11.01	9.21 (13.12)	9.24 (14.14)

[a] Isolated NO= 1.159 Å

[b] Expt: $\nu_{Isolated\ NO}$ = 1876 cm^{-1} $\Delta\nu_{Adsorbed\ NO}$ =+8 cm^{-1} (Hadjiivanov, 1998)

3. The interaction of a gold atom with carbon nanohorn and carbon nanotube tips and their complexes with a CO molecule

The structure of SWNH and SWNT tips were first performed as full optimizations. A C_{5V} symmetry point group had been chosen to constrain both systems during optimizations. Table 8 shows bond lengths, bond angles as well as the π-orbital axis vector (POAV) analysis for SWNH and SWNT tips. Even though they are rather analogous, the structures of both tips are to some extent dissimilar. The SWNT tip conserves the fullerene hemisphere geometric characteristics, as can be seen, a long-short-long-short pattern in bond lengths and 120-degree bond angles of six membered ring carbons whereas, in the SWNH tip, bond lengths and bond angles are rather altered from those in the fullerene hemisphere. The POAV analysis revealed some interesting results; the pyramidalization angle (θ_p) as well as π-orbital misalignment angles (ϕ) values in the SWNT tip are distributed in very short ranges, (11.7-12.0^o for θ_p and 0.0-1.0^o for ϕ), while those in the SWNH tip are uniquely different, (4.0-10.6^o for θ_p and 0.0-12.5^o for ϕ). For the SWNH tip case, it is noticed that C_1 has the highest θ_p (10.6^o) value. It can, therefore, be predicted that there would be many reactive carbon sites on the SWNT tip, but C_1 would be the only most favorable active site on the SWNH tip for such a chemical reaction.

Table 8 Geometric parameters (distances in pm. and angles in degrees), pyramidalization angles (θ_p) and π-orbital misalignment angles (ϕ) for the single-wall carbon nanohorn (SWNH) tip and the single-wall carbon nanotube (SWNT) tip systems.

	Geometric			**POAV Analysis**	
	NH Tip	**NT Tip**		**NH Tip**	**NT Tip**
Distances (pm)			θ_p **(deg)**		
C_1-C_2	142.9	145.8	θ_p (C_1)	10.6	11.9
C_1-C_6	140.2	140.9	θ_p (C_6)	5.6	12.0
C_6-C_7	143.8	145.3	θ_p (C_7)	4.0	11.7
C_7-C_8	143.6	140.2	ϕ **(deg)**		
Angles (deg)			ϕ (C_1-C_2)	0.0	0.0
C_1-C_2-C_3	108.0	108.0	ϕ (C_1-C_6)	0.0	0.0
C_2-C_1-C_6	121.0	119.8	ϕ (C_6-C_7)	12.5	1.0
C_1-C_6-C_7	118.3	120.1	ϕ (C_7-C_8)	0.0	0.0

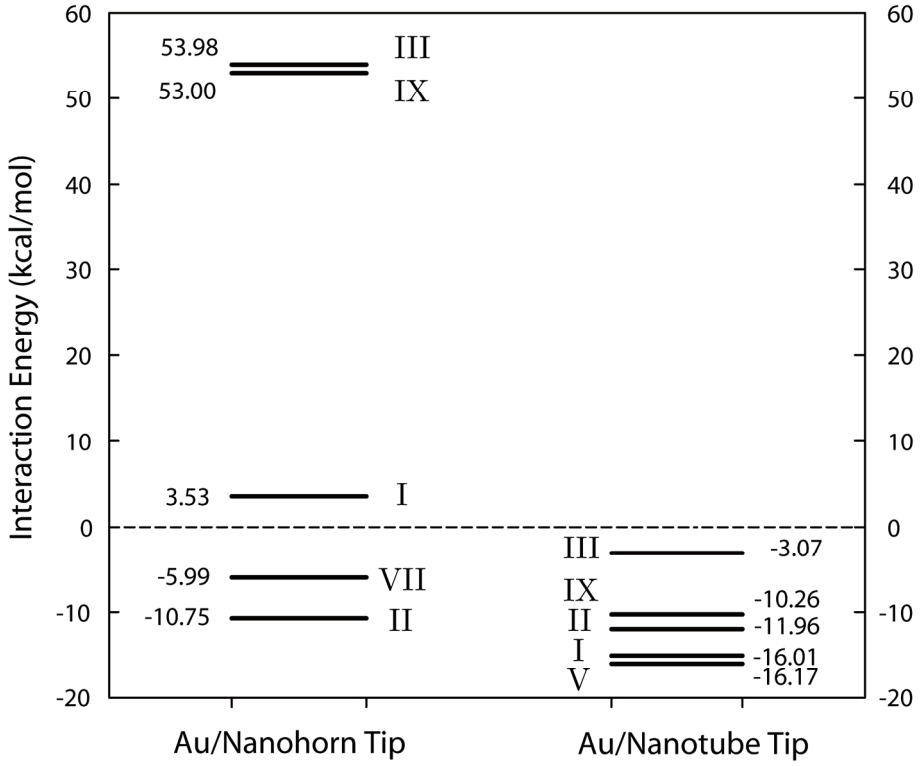

Figure 16 Interaction energy diagram for a gold atom adsorbed on the Nanohorn (SWNH) and Nanotube (SWNT) tips. Energies are in kcal/mol.

Although 9 different sites were probed with a gold atom on top of both tips, a certain number of them were found to be preferential binding sites for the gold atom. Figure 16 shows the comparison of interaction energies between the gold atom and the bind sites on top of the SWNH tip and the SWNT tip. The results from the interaction of the gold atom with both tips are totally different. Interaction of the gold atom on the SWNT tip has 5 local minima, and all of them are thermodynamically preferable, whereas only 2 of the 5 of the Au/SWNH tip complex are. The largest magnitude of interaction energy of -10.75 kcal/mol for the Au/SWNH tip complex is acquired from the di-coordinated site II. For the Au/SWNT tip complex, the gold atom binds tightest to the mono-coordinated site V with the interaction energy of -16.17 kcal/mol. The structural parameters of the gold atom on SWNH and SWNT tips are listed in Table 9. For the Au/SWNH tip complex, the gold atom is on the top of the bond between C_1-C_2 of the SWNH tip. Two equivalent Au-C_1 and Au-C_2 distances are evaluated to be 239.7 pm. At this state of interaction, the C_1-C_2 bond is lengthened from an isolated structure value of 142.9 pm to 146.3 pm. Smaller changes are observed for the bond lengths of C_1-C_6(1.6), C_6-C_7(-0.2) and C_7-C_8(0.4). The C_2-C_1-Au angle is measured to be 72.2^o. Unlike the Au/SWNH tip, the gold atom mono-coordinated locates on top of the C_6 atom with a distance of 214.4 pm. Certainly, C_1-C_6 bonds as well as the C_6-C_7 bond are lengthened by 5.6 and 4.5 pm, respectively. Besides, C_1-C_2 and C_7-C_8 bonds are slightly shortened by 1.2 and 0.5 pm, respectively. It is noted that the C_1-C_6-C_7 angle decreases from the aromaticity angle 120.1^o to 115.2^o, as well as that C_1-C_6-Au reveals an sp^3 characteristic angle of 107.3^o.

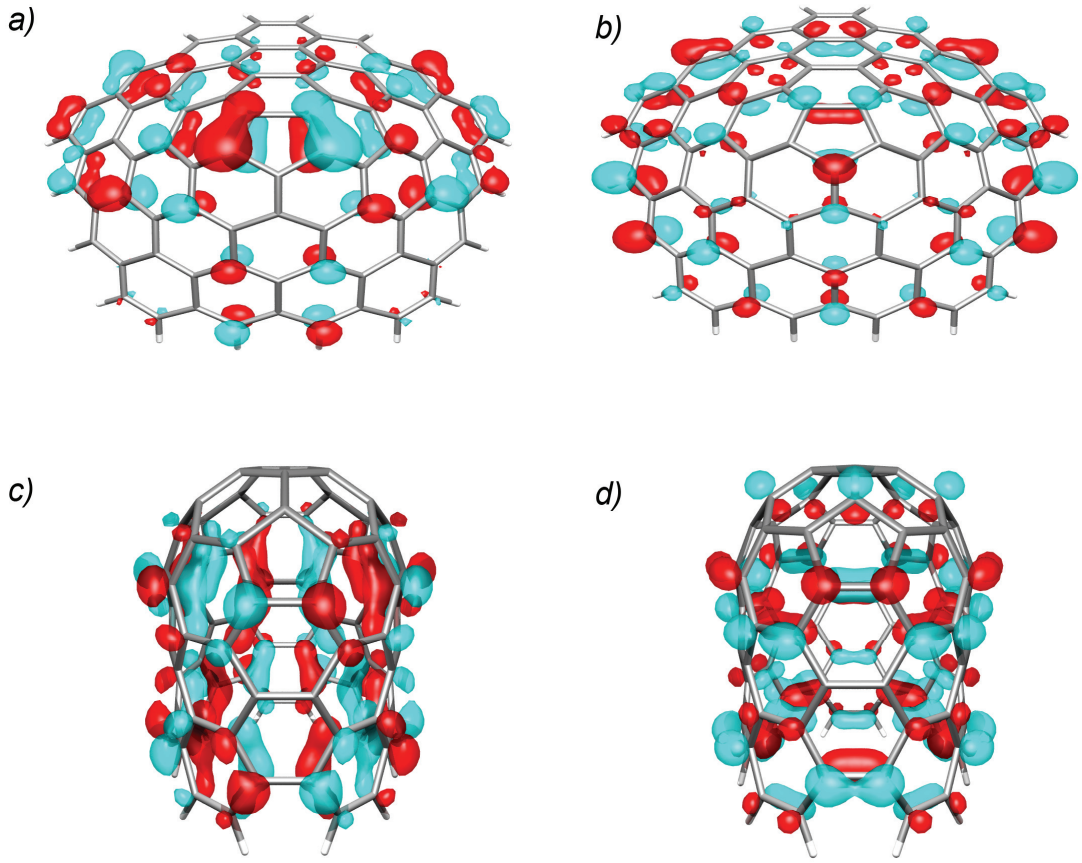

Figure 17 Molecular orbital plots for a) HOMO of SWNH tip, b) LUMO of SWNH tip, c) HOMO of SWNT tip, and d) LUMO of SWNT tip.

The cause of a high selectivity of gold on the top of the SWNH tip could be explained by the POAV analysis parameters (cf. Table 8). The SWNT tip has all large magnitudes of pyramidalization angles (θ_p) and all zeroes of π-orbital misalignment angles (ϕ), the gold atom can locate on several sites among the tip surface. For the SWNH tip, only C_1 has a largest value of θ_p, also the π-orbitals of C_1 and C_2 are well adjusted to each other (ϕ=0.0). Moreover, variations of θ_p angles and non-zero ϕ values cause a break down of the conjugated network on the SWNH tip. This leads to a specific binding of the gold atom on the bond between C_1 and C_2, known as site II. Further, to some degree, there is a correlation between the most stable location on the tip for the gold atom and the shape of the lowest unoccupied molecular orbital (LUMO) of the tip. Figure 17 shows the plots of the highest occupied molecular orbital (HOMO) and the lowest unoccupied molecular orbital (LUMO) for both SWNH and SWNT tips. From the fact that gold atoms possess positive charges in both cases of Au/SWNH and Au/SWNT complexes, a major contribution of a tip should come from the LUMO frontier orbital that is mainly responsible for an electron accepting process. It should be noted that there are some contributions from those carbons at the apex of the SWNH tip in the LUMO orbital, whereas for the SWNT tip, it is clearly seen that there is a lack of contribution from those carbon atoms (C_1-C_5) on the top of the tip. Among the apex area of the SWNT tip, C6 (site V) has the highest contribution on the LUMO orbital.

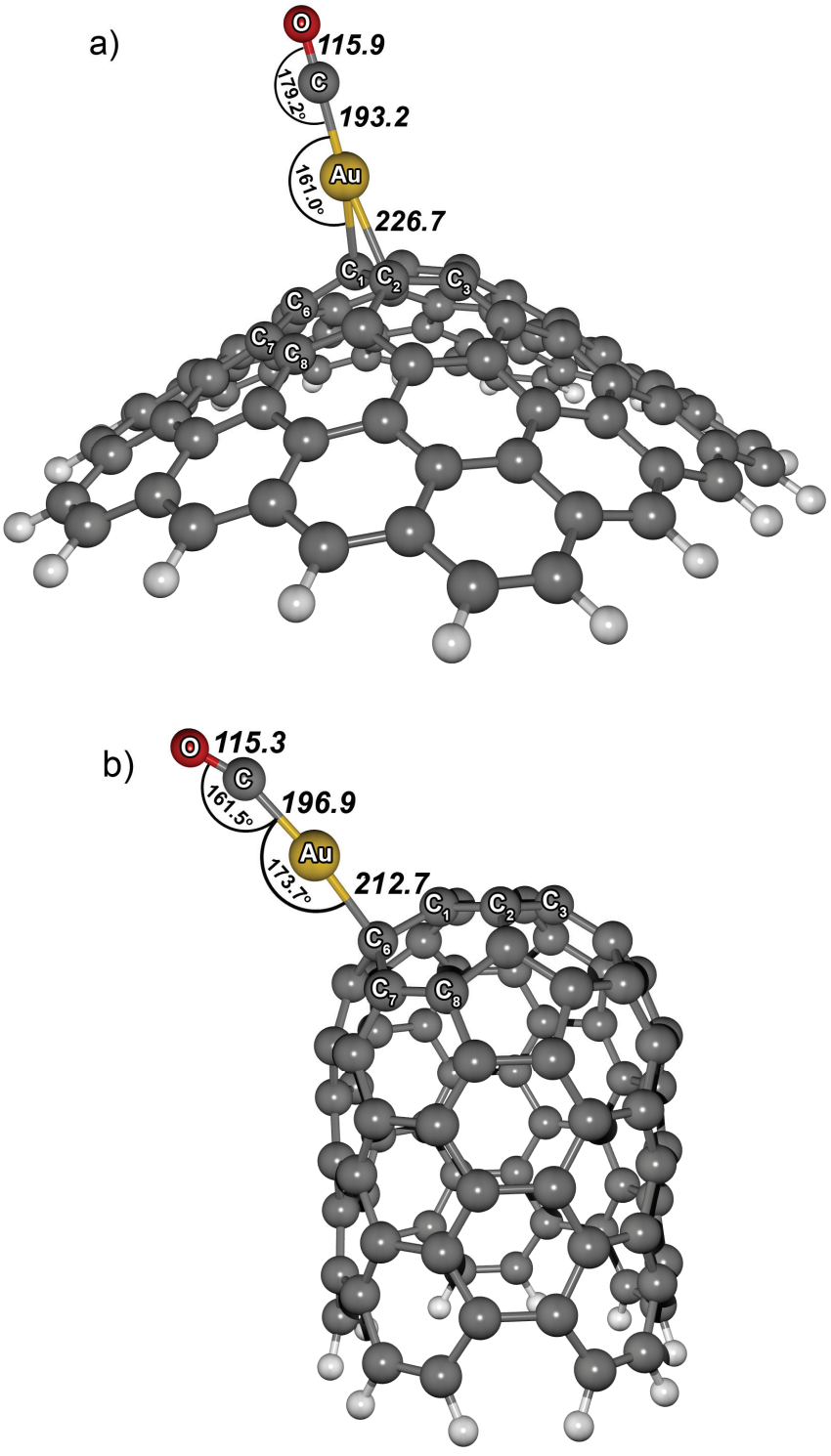

Figure 18 Interaction of the CO molecule with the gold atom on the top of a) Nanohorn tip and b) Nanotube tip, distances are shown in picometers and angles are shown in degrees.

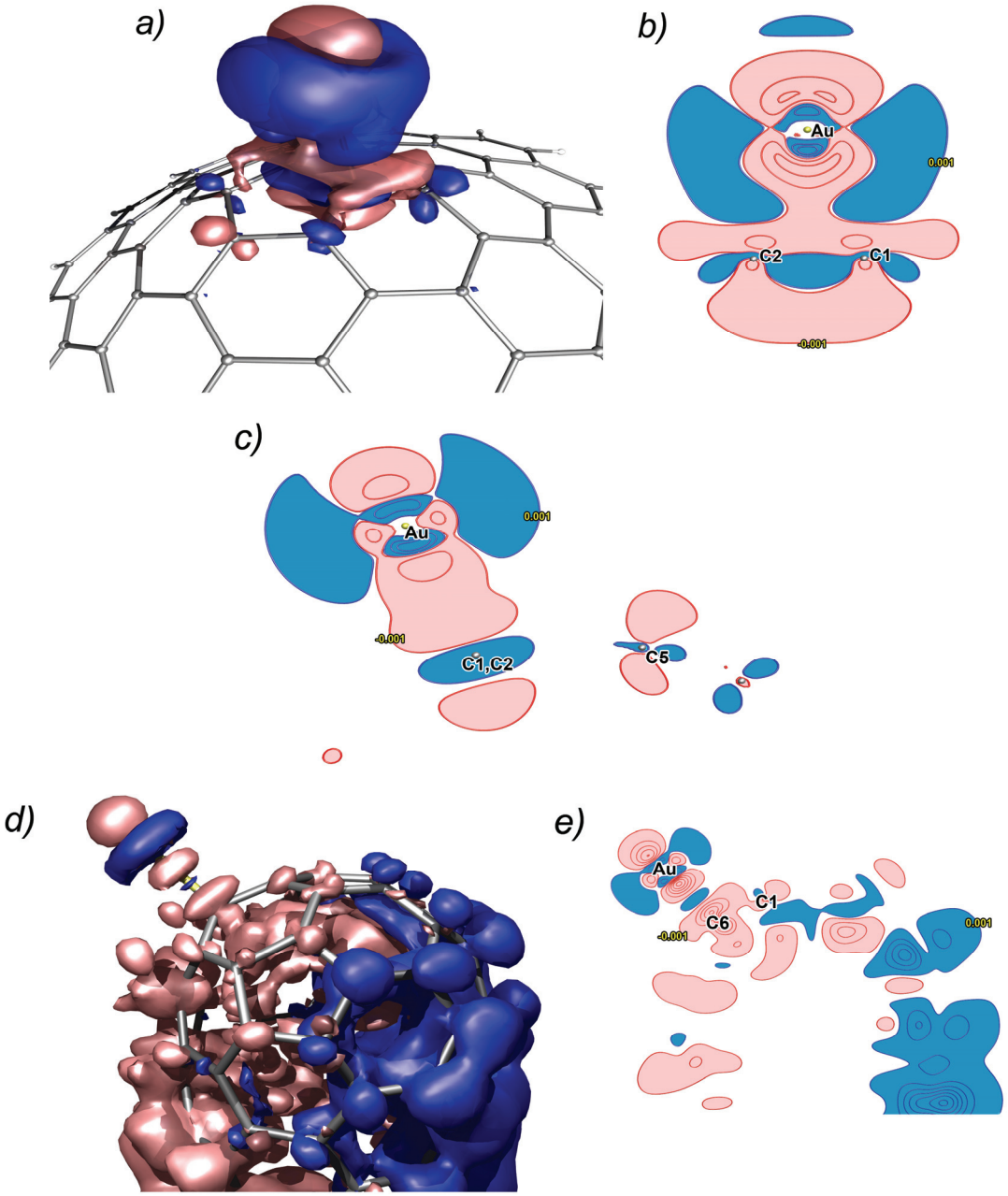

Figure 19 Electron density difference plots for a) Au---SWNH (3D) system b) Au---SWNH (2D) system on the plane that contains C_1,C_2, and Au atoms c) Au---SWNH (2D) system on the plane that cuts between C_1 and C_2 d) Au---SWNT (3D) system e) Au---SWNT (2D) system on the plane that contains C_1,C_6, and Au atoms. 3D plots use the isovalue = 0.001 e/Å^3. 2D plots start with isovalue = ±0.001 e/Å^3 and the interval = 0.01 e/Å^3. The blue area represents the electron accumulation while the pink region corresponds to the electron diminishing.

In order to distinguish between the reactivity of SWNH and SWNT tips, a carbon monoxide molecule was probed on the top of the gold atom at the most preferred site. Geometric parameters as well as binding energies for the interaction of CO with the gold atom on both SWNH and SWNT tips are tabulated in Table 9 and depicted in Figure 18. It was found that Au/SWNH and Au/SWNT systems have rather different binding characteristics. A CO molecule binds linearly with the Au atom on the SWNH tip with the Au-C-O angle of 179.1^{o}. The distance between CO and Au is found to be 193.2 pm. While only small changes are found on the structural parameters of the SWNH tip, the Au atom moves remarkably closer to the SWNH tip surface. The Au-C_1 distance is measured to be 226.6 pm, which is shortened by 13.1 pm through the approaching CO molecule. Unlike the Au/SWNH tip system, CO attacks the Au atom on the SWNT tip with a bent orientation. Au-C-O and C_6-Au-C angles (cf. Figure 18) are measured to be 161.5^{o} and 173.7^{o}, respectively. The distance between CO and Au is found to be 196.9 pm. A 1.7 pm shorter distance between the Au atom and C_6 of the SWNT tip surface is also found when a CO molecule is interacting on the Au atom. The interaction energies for the CO-Au/SWNH tip and CO-Au/SWNT tip are calculated to be -22.34 and -18.29 kcal/mol, respectively.

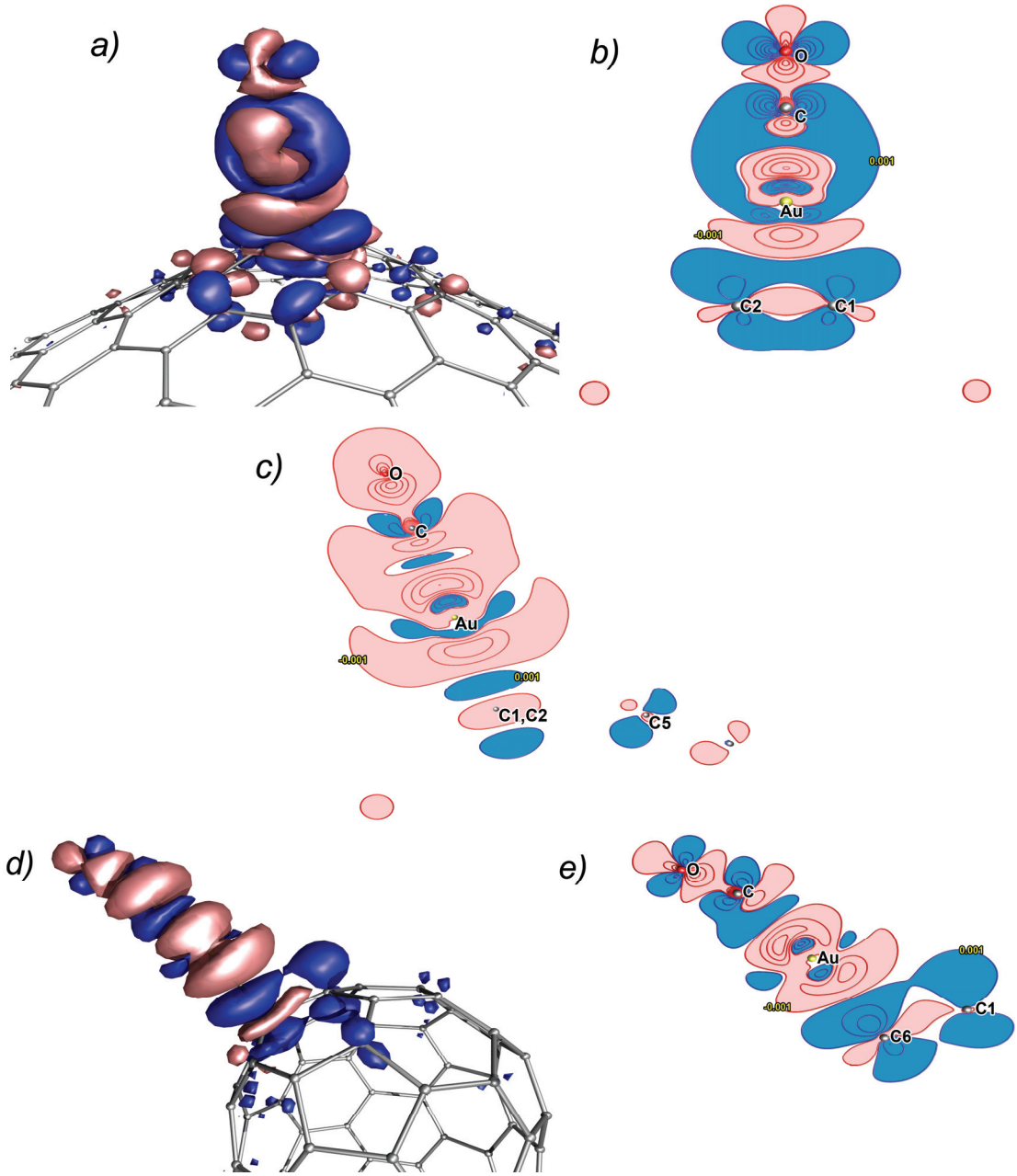

Figure 20 Electron density difference plots for a) CO---Au/SWNH (3D) system b) CO---Au/SWNH (2D) system on the plane that contains C_1,C_2, and Au atoms c) CO---Au/SWNH (2D) system on the plane that cuts between C_1 and C_2 d) CO---Au/SWNT (3D) system e) CO---Au/SWNT (2D) system on the plane that contains C_1,C_6, and Au atoms. 3D plots use the isovalue = 0.001 e/Å^3. 2D plots start with isovalue = ±0.001 e/Å^3 and use the interval = 0.01 e/Å^3. The blue area represents the electron accumulation while the pink region corresponds to the electron diminishing.

Table 9 Geometric parameters (distances in pm. and angles in degrees), natural population analysis charges (e) and binding energies (kcal/mol) for the interaction of a gold atom with the Nanohorn (SWNH) tip and the Nanotube (SWNT) tip.

	Au-NH Tip (II)	**Au-NT Tip (V)**	**CO···Au-NH Tip (II)**	**CO···Au-NT Tip (V)**
Distances (pm)				
C_1-C_2	146.3	144.6	147.7	144.5
C_1-C_6	141.8	146.5	143.2	148.8
C_6-C_7	143.6	149.8	142.5	150.4
C_7-C_8	144.0	139.7	145.6	139.5
C_n-Au	239.7	214.4	226.6	212.7
Au-C^{co}	-	-	193.2	196.9
C-O	-	-	115.9	115.3
Angles (deg)				
C_1-C_2-C_3	107.2	108.2	106.8	108.2
C_2-C_1-C_6	120.1	121.4	119.6	121.4
C_1-C_6-C_7	118.5	115.2	118.9	114.2
C_m-C_n-Au	72.2	107.3	71.0	100.1
C_n-Au-C^{co}	-	-	161.0	173.7
Au-C-O	-	-	179.1	161.5
NPA (e)				
q(Tip)	-0.08063	-0.12437	-0.52618	-0.50713
q(Au)	0.08063	0.12437	0.59114	0.47129
q(CO)	-	-	-0.06496	0.03584
Binding Energies (kcal/mol)				
ΔE(Au/Tip)	-10.75	-16.17	-	-
ΔE(CO/Au-Tip)	-	-	-22.34	-18.29

The characteristics of such interactions have been analyzed using the density difference procedures. Figure 19 shows the electron density difference plots for the interactions of the gold atom with the SWNH tip as well as with the SWNH tip. It is found that the electron density change due to the interaction of the gold atom on the SWNH tip occurs mostly in the apex area. The electron density redistribution infers that the gold atom is not only liberating electron density to the SWNH tip but also receiving it back via the □-back bonding from the C_1-C_2 bond, which could be observed from an electron density accumulation around the gold atom. Unlike the Au/SWNH tip, the electron density change in the Au/SWNT tip complex occurs definitely all over locations in the system. This behavior reveals the metal characteristic of the SWNT tip. A strong σ-donation (more negative contour lines) and a weak π-back bonding (less positive contour lines) interactions in the region of the gold atom are also found. These findings would support the strong interaction energy in the Au/SWNT tip complex.

The electron density difference technique was also applied in the interactions of the CO molecule with the gold atom located on both of the SWNH and SWNT tips. Figure 20 illustrates the electron density difference plots for the interactions of the CO molecule with both the Au/SWNH and Au/SWNT tips. The electron density difference plots indirectly imply that the CO molecule binds with the Au/SWNH tip via a strong ligand to metal σ-donation as well as having strong metal to ligand π -back bonding interactions, whereas there are both weaker ligand to metal σ-donation and weaker metal to ligand π -back bonding interactions found in the CO---Au/SWNT tip complex. Moreover, the metal to ligand π-back bonding is too weak to maintain a state of equilibrium on both sides of the π* character of the CO molecule and causes a bent configuration of the adsorbed CO molecule on the Au/SWNT tip. It needs to be remarked that both σ-donation and π-back bonding interactions between the CO molecule and the gold atom would make a lower bond order in the CO molecule. Consequentially, there is a correlation between the CO distance and an interaction of the CO molecule and the gold atom. The higher the CO-Au interaction energy, the longer the C-O bond length is.

From consideration of the electronic levels of molecular orbitals in the systems, it is found that the SWNH tip has a HOMO-LUMO energy gap of 1.50 eV. For the Au/SWNH tip system, the electronic state contribution from the Au atom alters the HOMO-LUMO energy gap to become 0.70 eV, while the CO molecule adsorbed on the top of the Au atom, the energy gap is finally changed to become 0.07 eV. In the case of the SWNT tip, it shows a metallic nature with a 1.16 eV HOMO-LUMO energy gap, whilst for the Au/SWNT tip system, the energy gap is changed to 0.99 eV. In respect of the interaction of the CO molecule with the Au/SWNT tip, the energy gap is evaluated to be 0.63 eV.

Table 10 Electronic HOMO-LUMO energy gap (eV) for the Nanohorn (SWNH) and the Nanotube (SWNT) tip as well as their Au complexes with CO molecules.

	SWNH Tip	**SWNT Tip**
Tip	**1.50**	**1.16**
Tip-Au	**0.70**	**0.99**
Tip-Au-CO	**0.07**	**0.63**

CONCLUSIONS

1. Adsorption of CO in H-ZSM-5 and Li-ZSM-5 zeolites

The absorption of carbon monoxide with H-ZSM-5 and metal-substituted Li-ZSM-5 zeolites has been investigated by using both cluster and embedded cluster approaches. For the H-ZSM-5 zeolite, the binding energy of CO on a 3T quantum cluster is predicted to be 2.25 kcal/mol for the C-bound complex. The O-bound complex was found to be less stable by about 0.84 kcal/mol. Inclusion of the Madelung potential was found to increase the acidity of the Brønsted acidic site and the CO-binding energy to 4.95 kcal/mol, consequently, it leads better agreement with experimental observation. Similar results were also obtained for the Li-ZSM-5rCO complex. The Madelung potential field from the zeolite framework was found to reverse the order of relative stability of C-bound and O-bound adducts.

The interactions of CO with H-FAU and metal-exchange Li-FAU zeolites have also been investigated by means of cluster and embedded cluster approaches. In the case of the protonated zeolite, the adsorption energy of the bare quantum cluster is evaluated to be -1.90 kcal/mol for the H-FAU/CO complex. Inclusion of the Madelung potential field from the zeolite framework has an effect of lengthening the OH distance, hence enhancing the binding energies of the H-FAU/CO (-3.20 kcal/mol). For adsorption of CO on the metal-exchanged zeolites, the Madelung potential was found to differentiate the different types of zeolites (ZSM-5 and FAU), that cannot be drawn from the typical 3T quantum cluster. This finding clearly demonstrates that acidity does not depend only on the Brønsted group center, but also on the dimension of the channel where the Brønsted group is located. The adsorption energy of the embedded cluster model (-6.69 kcal/mol) lies between those of the bare quantum cluster model (-5.81 kcal/mol) and the simple naked Li^+/CO system (-13.14 kcal/mol). Correction of the 3T cluster model to take into account the long range contribution of the electrostatic potential of the zeolite crystal is found to agree with the experimental observation.

2. Adsorption of NO and CO on Ag-ZSM-5

The electronic embedded density functional theory was employed to study adsorption of NO and CO on Ag-ZSM-5 zeolite. Our predicted structures and energetics agree very well with those observed from experiments. The dependence on the cluster size and the Madelung potential suggest not only the Madelung potential is necessary but also a sufficiently large cluster must be used for modeling adsorption properties quantitatively. A large blue-shift of adsorbed CO stretching mode predicted in this study ($\Delta\nu$=55.2 cm^{-1}) confirms the experimental observation ($\Delta\nu$=48 cm^{-1}). Despite a shorter NO bond length, I obtained a slight red-shift of NO stretching model, instead of slight blue-shift ($\Delta\nu$ = 6 to 8 cm^{-1}) found by experiments. Including the Madelung potential shifts the frequency by as much as 30 cm^{-1} to get closer to the experimental blue-shifted NO frequency. This suggests that the lattice effect is important in study adsorption on zeolite.

The binding energy of CO/Ag-ZSM-5 complex of 18.63 kcal/mol is substantially larger than that of NO/Ag-ZSM-5 (9.24 kcal/mol). Comparing to the Cu-ZSM-5 zeolite, CO and NO adsorption on Ag-ZSM-5 has much smaller binding energy. This lower binding energy between Ag-ZSM-5 and small adsorbates compared to that of Cu-ZSM-5 may relate to the higher catalytic reactivity of Ag-ZSM-5 in NO decomposition.

3. Interaction of a gold atom with carbon nanohorn and carbon nanotube tips and their complexes with a CO molecule

Both carbon nanohorn and carbon nanotube tips are carbon nanostructure compounds, which are derived from a graphene sheet pattern. Despite, the topologies of the top surfaces of both systems being quite similar, their electronic and chemical properties are entirely different. The geometrical structure of the SWNT tip shows fullerene hemisphere characteristics but bond lengths and bond angles in the SWNH tip are rather different. The results from the pyramidalization angle (θ_p) as well as the

π-orbital misalignment angle (ϕ), the analysis of which leads to a prediction that there would be many reactive carbon sites on the SWNT tip and C_1 would be the only most favorable active site on the SWNH tip. It is consequently found that only five locations on SWNT are proper for being attached by the gold atom. Despite the fact that there are also five local minima found for the Au/SWNH tip complex, only two of them are thermodynamically favored. The interaction of the gold atom at the di-coordinated site II on the SWNH tip has the largest interaction energy of -10.75 kcal/mol. For the Au/SWNT tip complex, the gold atom binds tightest to the mono-coordinated site V with the interaction energy of -16.17 kcal/mol. The high selectivity of the SWNH tip and no specificity of the SWNT tip behavior in the interaction with the gold atom corresponds well with the prior POAV expectation.

Both the Au/SWNH tip and Au/SWNT tip systems had been probed by the CO molecule and it was found that the CO molecule binds with the Au/SWNH tip (site II) and the Au/SWNT tip (site V) with the interaction energies -22.34 and -18.29 kcal/mol, respectively. By taking advantage of the electronic density difference plot, it reveals that the σ-donation as well as π-back bonding interactions on the gold atom are the major factors on the property of those complexes of the gold atom with SWNH and SWNT tips. The CO molecule binds tightly with Au/SWNH tip by both strong σ-donation and strong π-back bonding interactions causing a linearly alignment of the CO and the gold atom on the SWNH tip. The electronic characteristics of both the Au/SWNH and Au/SWNT tips are very sensitive upon an adsorption of the CO molecule. The changes of the energy gap due to an interaction of the CO molecule on the Au/SWNH and the Au/SWNT tip systems are 0.63 eV and 0.36 eV, respectively.

LITERATURE CITED

Ahlrichs, R., M. Baer, M. Haeser, H. Horn and C. Koelmel. 1989. Electronic structure calculations on workstation computers: the program system TURBOMOLE. **Chem. Phys. Lett.** 162(3):165-169.

Ajima, K., M. Yudasaka, T. Murakami, A. Maigne, K. Shiba and S. Iijima. 2005. Carbon Nanohorns as Anticancer Drug Carriers. **Mol. Pharma.** 2(6):475-480.

Allavena, M., K. Seiti, E. Kassab, G. Ferenczy and J.G. Angyan. 1990. Quantum-chemical model calculations on the acidic site of zeolites including Madelung-potential effects. **Chem. Phys. Lett.** 168461-467.

Anpo, M. 1997. Photocatalysis on titanium oxide catalysts. Approaches in achieving highly efficient reactions and realizing the use of visible light. **Catal. Surv. Jap.** 1(2):169-179.

Astala, R. and S.M. Auerbach. 2004. The Properties of Methylene- and Amine-Substituted Zeolites from First Principles. **J. Am. Chem. Soc.** 126(6):1843-1848.

_____, S.M. Auerbach and P.A. Monson. 2004. Density Functional Theory Study of Silica Zeolite Structures: Stabilities and Mechanical Properties of SOD, LTA, CHA, MOR, and MFI. **J. Phys. Chem. B** 108(26):9208-9215.

Bates, S. and J. Dwyer. 1993. Ab initio study of carbon monoxide adsorption on zeolites. **J. Phys. Chem.** 97(22):5897-5900.

Becke, A.D. 1986. Density functional calculations of molecular bond energies. **J. Chem. Phys.** 84(8):4524-4529.

_____. 1993. Density Functional Thermochemistry. III. The Role of Exact Exchange. **J. Chem. Phys.** 98(7):5648-5652.

Bekyarova, E., K. Murata, M. Yudasaka, D. Kasuya, S. Iijima, H. Tanaka, H. Kahoh and K. Kaneko. 2003. Single-Wall Nanostructured Carbon for Methane Storage. **J. Phys. Chem. B** 107(20):4681-4684.

Bell, A.T. 1997. Experimental and theoretical studies of NO decomposition and reduction over metal-exchanged ZSM-5. **Catal. Today** 38(2):151-156.

Blaszkowski, S.R. and R.A. van Santen. 1995. Density Functional Theory Calculations of the Activation of Methanol by a Broensted Zeolitic Proton. **J. Phys. Chem.** 99(30):11728-11738.

Bordiga, S., E. Escalona Platero, C. Otero Arean, C. Lamberti and A. Zecchina. 1992. Low temperature carbon monoxide adsorption on Na-ZSM-5 zeolites: an FTIR investigation. **J. Catal.** 137(1):179-185.

_____, E. Garrone, C. Lamberti, A. Zecchina, C.O. Arean, V.B. Kazansky and L.M. Kustov. 1994. Comparative IR-spectroscopic study of low-temperature H2 and CO adsorption on Na zeolites. **J. Chem. Soc., Faraday Trans.** 90(21):3367-3372.

_____, D. Scarano, G. Spoto, A. Zecchina, C. Lamberti and C. Otero Arean. 1993. Infrared study of carbon monoxide adsorption at 77 K on faujasites and ZSM 5 zeolites. **Vib. Spectrosc.** 5(1):69-74.

Boronat, M., C.M. Zicovich-Wilson, P. Viruela and A. Corma. 2001. Influence of the Local Geometry of Zeolite Active Sites and Olefin Size on the Stability of Alkoxide Intermediates. **J. Phys. Chem. B** 105(45):11169-11177.

Boys, S.F. and F. Bernardi. 1970. BSSE CP. **Mol. Phys.** 19553.

Brandle, M. and J. Sauer. 1997. Combining ab initio techniques with analytical potential functions. A study of zeolite—adsorbate interactions for NH3 on H-faujasite. **J. Mol. Catal. A** 11919-33.

_____. 1998. Acidity Differences between Inorganic Solids Induced by Their Framework Structure. A Combined Quantum Mechanics/Molecular Mechanics ab Initio Study on Zeolites. **J. Am. Chem. Soc.** 120(7):1556-1570.

_____, R. Dovesi and N.M. Harrison. 1998. Comparison of a combined quantum mechanics/interatomic potential function approach with its periodic quantum-mechanical limit: Proton siting and ammonia adsorption in zeolite chabazite. **J. Chem. Phys.** 109(23):10379-10389.

Bredow, T., G. Geudtner and K. Jug. 1996. Embedding procedure for cluster calculations of ionic crystals. **J. Chem. Phys.** 1056395-6400.

Bronstein, H.E., N. Choi and L.T. Scott. 2002. Practical Synthesis of an Open Geodesic Polyarene with a Fullerene-type 6:6-Double Bond at the Center: Diindeno[1,2,3,4-defg;1',2',3',4'-mnop]chrysene. **J. Am. Chem. Soc.** 124(30):8870-8875.

Campana, L., A. Selloni, J. Weber, A. Pasquarello, I. Papai and A. Goursot. 1994. First principles molecular dynamics calculation of the structure and acidity of a bulk zeolite. **Chem. Phys. Lett.** 226(3-4):245-250.

Cao, A., H. Zhu, X. Zhang, X. Li, D. Ruan, C. Xu, B. Wei, J. Liang and D. Wu. 2001. Hydrogen storage of dense-aligned carbon nanotubes. **Chem. Phys. Lett.** 342(5-6):510-514.

Charlier, J.C. and G.M. Rignanese. 2001. Electronic structure of carbon nanocones. **Phys. Rev. Lett.** 86(26 Pt 1):5970-5973.

Chen, N. and R.T. Yang. 1996. Ab Initio Molecular Orbital Study of Adsorption of Oxygen, Nitrogen, and Ethylene on Silver-Zeolite and Silver Halides. **Ind. Eng. Chem. Res.** 35(11):4020-4027.

Chu, C.T.W. and C.D. Chang. 1985. Isomorphous substitution in zeolite frameworks. 1. Acidity of surface hydroxyls in [B]-, [Fe]-, [Ga]-, and [Al]-ZSM-5. **J. Phys. Chem.** 89(9):1569-1571.

Civalleri, B., P. D'Arco, R. Orlando, V.R. Saunders and R. Dovesi. 2001. Hartree-Fock geometry optimisation of periodic systems with the CRYSTAL code. **Chem. Phys. Lett.** 348(1,2):131-138.

Collins, P.G. and P. Avouris. 2000. Nanotubes for electronics. **Scientific American** 283(6):62-69.

Damin, A., F. Bonino, G. Ricchiardi, S. Bordiga, A. Zecchina and C. Lamberti. 2002a. Effect of NH3 Adsorption on the Structural and Vibrational Properties of TS-1. **J. Phys. Chem. B** 106(30):7524-7526.

_____, S. Bordiga, A. Zecchina and C. Lamberti. 2002b. Reactivity of Ti(IV) sites in Ti-zeolites: An embedded cluster approach. **J. Chem. Phys.** 117(1):226-237.

Dandekar, A. and M.A. Vannice. 1999. Decomposition and reduction of N2O over copper catalysts. **App. Catal. B: Env.** 22(3):179-200.

Dapprich, S., I. Komiromi, K.S. Byun, K. Morokuma and M.J. Frisch. 1999. A new ONIOM implementation in Gaussian98. Part I. The calculation of energies, gradients, vibrational frequencies and electric field derivatives. **J. Mol. Struc. (THEOCHEM)** 461-4621-21.

Dartt, C.B. and M.E. Davis. 1994. Applications of zeolites to fine chemicals synthesis. **Catal. Today** 19(1):151-186.

Das, J., C.V.V. Satyanaryana, D.K. Chakrabarty, S.N. Piramanayagam and S.N. Shringi. 1992. Substitution of aluminum in the AlPO4-5 and AlPO4-11 frameworks by silicon and iron: a study by Moessbauer, magic-angle-spinning nuclear magnetic resonance and electron paramagnetic resonance spectroscopies and chemical probes. **J. Chem. Soc., Faraday Trans.** 88(21):3255-3261.

Dixon, D.A., J.L. Gole and A. Komornicki. 1988. Lithium and sodium cation affinities of hydrogen, nitrogen, and carbon monoxide. **J. Phys. Chem.** 92(5):1378-1382.

Eichkorn, K., O. Treutler, H. Oehm, M. Haeser and R. Ahlrichs. 1995. Auxiliary basis sets to approximate Coulomb potentials. **Chem. Phys. Lett.** 240(4):283-290.

Ferrari, A.M., K.M. Neyman and N. Roesch. 1997. CO Interaction with Alkali Metal Cations in Zeolites: A Density Functional Model Cluster Study. **J. Phys. Chem. B** 101(45):9292-9298.

_____, P. Ugliengo and E. Garrone. 1996. Ab initio study of the adducts of carbon monoxide with alkaline cations. **J. Chem. Phys.** 105(10):4129-4139.

Franklin, N.R., Q. Wang, T.W. Tombler, A. Javey, M. Shim and H. Dai. 2002. Integration of suspended carbon nanotube arrays into electronic devices and electromechanical systems. **Appl. Phys. Lett.** 81(5):913-915.

Frisch, M.J., G.W. Trucks, H.B. Schlegel, G.E. Scuseria, M.A. Robb, J.R. Cheeseman, J. Montgomery, J. A., T. Vreven, K.N. Kudin, J.C. Burant, J.M. Millam, S.S. Iyengar, J. Tomasi, V. Barone, B. Mennucci, M. Cossi, G. Scalmani, N. Rega, G.A. Petersson, H. Nakatsuji, M. Hada, M. Ehara, K. Toyota, R. Fukuda, J. Hasegawa, M. Ishida, T. Nakajima, Y. Honda, O. Kitao, H. Nakai, M. Klene, X. Li, J.E. Knox, H.P. Hratchian, J.B. Cross, V. Bakken, C. Adamo, J. Jaramillo, R. Gomperts, R.E. Stratmann, O. Yazyev, A.J. Austin, R. Cammi, C. Pomelli, J.W. Ochterski, P.Y. Ayala, K. Morokuma, G.A. Voth, P. Salvador, J.J. Dannenberg, V.G. Zakrzewski, S. Dapprich, A.D. Daniels, M.C. Strain, O. Farkas, D.K. Malick, A.D. Rabuck, K. Raghavachari, J.B. Foresman, J.V. Ortiz, Q. Cui, A.G. Baboul, S. Clifford, J. Cioslowski, B.B. Stefanov, G. Liu, A. Liashenko, P. Piskorz, I. Komaromi, R.L. Martin, D.J. Fox, T. Keith, M.A. Al-Laham, C.Y. Peng, A. Nanayakkara, M. Challacombe, P.M.W. Gill, B. Johnson, W. Chen, M.W. Wong, C. Gonzalez and J.A. Pople. 2004. **Gaussian 03, Revision B.05,** Gaussian, Inc., Wallingford, CT.

Giamello, E., D. Murphy, G. Magnacca, C. Morterra, Y. Shioya, T. Nomura and M. Anpo. 1992. The interaction of nitric oxide with copper ions in ZSM5: an EPR and IR investigation. **J. Catal.** 136(2):510-520.

Gonzales, N.O., A.T. Bell and A.K. Chakraborty. 1997. Density Functional Theory Calculations of the Effects of Local Composition and Defect Structure on the Proton Affinity of H-ZSM-5. **J. Phys. Chem. B** 101(48):10058-10064.

Gooding, J.J. 2005. Nanostructuring electrodes with carbon nanotubes: A review on electrochemistry and applications for sensing. **Electrochim. Acta** 50(15):3049-3060.

Greatbanks, S.P., P. Sherwood and I.H. Hillier. 1994. Embedded Cluster Model for the ab Initio Study of Broensted Acidity in Zeolites. **J. Phys. Chem.** 98(33):8134-8139.

Hadjiivanov, K.I. 1998. IR study of CO and NOx sorption on Ag-ZSM-5. **Microporous Mesoporous Mater.** 24(1-3):41-49.

_____, M.M. Kantcheva and D.G. Klissurski. 1996. IR study of CO adsorption on Cu-ZSM-5 and CuO/SiO2 catalysts: s and p components of the Cu+-CO bond. **J. Chem. Soc., Faraday Trans.** 92(22):4595-4600.

Hass, K.C. and W.F. Schneider. 1996. Reliability of Small Cluster Models for Cu-Exchanged Zeolites. **J. Phys. Chem.** 100(22):9292-9301.

Hill, J.-R., C.M. Freeman and B. Delley. 1999. Bridging Hydroxyl Groups in Faujasite: Periodic vs Cluster Density Functional Calculations. **J. Phys. Chem. A** 103(19):3772-3777.

Hillier, I.H. 1999. Chemical reactivity studied by hybrid QM/MM methods. **J. Mol. Struc. (THEOCHEM)** 463(1-2):45-52.

Iijima, S., M. Yudasaka, R. Yamada, S. Bandow, K. Suenaga, F. Kokai and K. Takahashi. 1999. Nano-aggregates of single-walled graphitic carbon nano-horns. **Chem. Phys. Lett.** 309(3,4):165-170.

Ikuta, S. 1984. Ab initio MO calculations on the stable structures and binding energies of X+-carbon monoxide and X+-molecular nitrogen ions (X = H, Li, Na and K). **Chem. Phys. Lett.** 109(6):550-553.

_____. 1985. Ab initio MO calculations on the stable conformations and their binding energies of the ion-molecule complexes: ion = proton, lithium(1+), sodium(1+), potassium(1+), beryllium(2+), magnesium(2+), and calcium(2+); molecule = carbon monoxide and molecular nitrogen. **Chem. Phys.** 95(2):235-242.

Iwamoto, M., H. Furukawa, Y. Mine, F. Uemura, S. Mikuriya and S. Kagawa. 1986. Copper(II) ion-exchanged ZSM-5 zeolites as highly active catalysts for direct and continuous decomposition of nitrogen monoxide. **J. Chem. Soc., Chem. Commun.** (16):1272-1273.

Jeanvoine, Y., J.G. Angyan, G. Kresse and J. Hafner. 1998. Brønsted Acid Sites in HSAPO-34 and Chabazite: An Ab Initio Structural Study. **J. Phys. Chem. B** 102(29):5573-5580.

Kanan, S.M., M.A. Omary, H.H. Patterson, M. Matsuoka and M. Anpo. 2000. Characterization of the Excited States Responsible for the Action of Silver(I)-Doped ZSM-5 Zeolites as Photocatalysts for Nitric Oxide Decomposition. **J. Phys. Chem. B** 104(15):3507-3517.

Kanougi, T., K.-i. Furukawa, M. Yamadaya, Y. Oumi, M. Kubo, A. Stirling, A. Fahmi and A. Miyamoto. 1997. NO2 adsorption on ion exchanged ZSM-5: a density functional study. **Appl. Surf. Sci.** 119(1/2):103-106.

Kassab, E., J. Fouquet, M. Allavena and E.M. Evleth. 1993. Ab initio study of proton-transfer surfaces in zeolite models. **J. Phys. Chem.** 97(35):9034-9039.

Katoh, M., T. Yamazaki, H. Kamijo and S. Ozawa. 1995. Infrared studies on nitrogen oxides adsorbed on alkali metal ion-exchanged ZSM-5 zeolites. **Zeolites** 15(7):591-596.

Khaliullin, R.Z., A.T. Bell and V.B. Kazansky. 2001. An Experimental and Density Functional Theory Study of the Interactions of CH4 with H-ZSM-5. **J. Phys. Chem. A** 105(45):10454-10461.

Klamt, A. and G. Schuurmann. 1993. Cosmo - A New Approach to Dielectric Screening in Solvents with Explicit Expressions for the Screening Energy and Its Gradient. **Journal of the Chemical Society-Perkin Tranactions** 2(5):799-805.

Klinowski, J. 1991. Solid-state NMR studies of molecular sieve catalysts. **Chem. Rev.** 91(7):1459-1479.

Knozinger, H. and S. Huber. 1998. IR spectroscopy of small and weakly interacting molecular probes for acidic and basic zeolites. **J. Chem. Soc., Faraday Trans.** 94(15):2047-2059.

Kohn, W., A.D. Becke and R.G. Parr. 1996. Density Functional Theory of Electronic Structure. **J. Phys. Chem.** 100(31):12974-12980.

_____ and L.J. Sham. 1965. Self-Consistent Equations Including Exchange and Correlation Effects. **Phys. Rev.** 140(4 A):A 1133-A 1138.

Koszinowski, K., D. Schroeder, H. Schwarz, M.C. Holthausen, J. Sauer, H. Koizumi and P.B. Armentrout. 2002. Bond Dissociation Energies and Structures of CuNO+ and Cu(NO)2+. **Inorg. Chem.** 41(22):5882-5890.

Kramer, G.J., R.A. van Santen, C.A. Emeis and A.K. Nowak. 1993. Understanding the acid behavior of zeolites from theory and experiment. **Nature** 363(6429):529-531.

Kresse, G. and J. Furthmueller. 1996. Efficient iterative schemes for ab initio total-energy calculations using a plane-wave basis set. **Phys. Rev. B: Condens. Matter** 54(16):11169-11186.

Kriegl, J.M., K. Nienhaus, P. Deng, J. Fuchs and G.U. Nienhaus. 2003. Ligand dynamics in a protein internal cavity. **Proc. Natl. Acad. Sci. U. S. A.** 100(12):7069-7074.

Krossner, M. and J. Sauer. 1996. Interaction of Water with Broensted Acidic Sites of Zeolite Catalysts. Ab Initio Study of 1:1 and 2:1 Surface Complexes. **J. Phys. Chem.** 100(15):6199-6211.

Kubo, Y. 2002. Tiny fuel cells with carbon nanohorn electrodes. **Mater. Integrat.** 15(6):9-13.

_____. 2004. Micro fuel cells using carbon nanohorns. **Mater. Integrat.** 17(6):29-33.

Lai, D., J. Li, P. Huang and D. Wang. 1994. Ethanol oxidation to acetaldehyde over Ag-ZSM-5 zeolite. **J. Nat. Gas Chem.** 3(2):211-218.

Lamberti, C., S. Bordiga, F. Geobaldo, A. Zecchina and C. Otero Arean. 1995. Stretching frequencies of cation-CO adducts in alkali-metal exchanged zeolites: an elementary electrostatic approach. **J. Chem. Phys.** 103(8):3158-3165.

Larin, A.V. and D.P. Vercauteren. 2001. Lower order atomic multipole moments of the oxygen atoms of 'small size' H-form aluminocilicate frameworks. **J. Mol. Catal. A** 168123-138.

Lee, C., W. Yang and R.G. Parr. 1988. Development of the Colle-Salvetti correlation-energy formula into a functional of the electron density. **Phys. Rev. B: Condens. Matter** 37(2):785-789.

Lercher, J.A., C. Gruendling and G. Eder-Mirth. 1996. Infrared studies of the surface acidity of oxides and zeolites using adsorbed probe molecules. **Catal. Today** 27(3-4):353-376.

Li, X., H. Zhu, C. Xu, Z. Mao and D. Wu. 2003. Measuring hydrogen storage capacity of carbon nanotubes by tangent-mass method. **Int. J. Hydrogen Energy** 28(11):1251-1253.

Li, Z. and M. Flytzani-Stephanopoulos. 1999. On the Promotion of Ag-ZSM-5 by Cerium for the SCR of NO by Methane. **J. Catal.** 182(2):313-327.

Limtrakul, J., T. Nanok, S. Jungsuttiwong, P. Khongpracha and T.N. Truong. 2001. Adsorption of unsaturated hydrocarbons on zeolites: the effects of the zeolite framework on adsorption properties of ethylene. **Chem. Phys. Lett.** 349(1,2):161-166.

Lin, Y., F. Lu, Y. Tu and Z. Ren. 2004. Glucose biosensors based on carbon nanotube nanoelectrode ensembles. **Nano Letters** 4(2):191-195.

Makarova, M.A., S.P. Bates and J. Dwyer. 1995. In Situ Modeling of the Enhanced Broensted Acidity in Zeolites. **J. Am. Chem. Soc.** 117(45):11309-11313.

Martinez-Magadan, J.M., A. Cuan and M. Castro. 2002. An embedded QM/MM study for different SiO2/Al2O3 ratios of the HZSM-5 zeolite and for their interaction with N-heptane. **Int. J. Quantum Chem.** 88(6):750-766.

Maseras, F. and K. Morokuma. 1995. IMOMM: a new integrated ab initio + molecular mechanics geometry optimization scheme of equilibrium structures and transition states. **J. Comput. Chem.** 16(9):1170-1179.

Matsuoka, M., W.-S. Ju and M. Anpo. 2000. Photocatalytic decomposition of N2O into N2 and O2 on the silver(I) ion-exchanged ZSM-5 catalyst. **Chem. Lett.** (6):626-627.

_____, E. Matsuda, K. Tsuji, H. Yamashita and M. Anpo. 1996. The photocatalytic decomposition of nitric oxide on Ag+/ZSM-5 catalyst prepared by ion-exchange. **J. Mol. Catal. A** 107(1-3):399-403.

Muller, W. and P.S. Bagus. 1987. A comparison of the interaction of carbon monoxide, nitrogen, and oxygen-bonded carbon monoxide with copper(100). **J. Vac. Sci. Technol., A** 5(4, Pt. 2):1053-1056.

Murata, K., K. Kaneko, F. Kokai, K. Takahashi, M. Yudasaka and S. Iijima. 2000. Pore structure of single-wall carbon nanohorn aggregates. **Chem. Phys. Lett.** 331(1):14-20.

_____, J. Miyawaki, M. Yudasaka, S. Iijima and K. Kaneko. 2005. High-density of methane confined in internal nanospace of single-wall carbon nanohorns. **Carbon** 43(13):2826-2830.

_____, M. Yudasaka, S. Iijima, M. El-Merraoui and K. Kaneko. 2002. Classification of supercritical gas adsorption isotherms based on fluid-fluid interaction. **J. Appl. Phys.** 91(12):10227-10229.

_____ and K. Kaneko. 2003. Carbon nano-horn capable of storing high density methane. **Kogyo Zairyo** 51(4):77-80.

Nachtigall, P. and D. Nachtigallova. 2000. Coordination Charge of Cu+ Sites in ZSM-5 on Excitation in the Triplet State: Understanding of the Photoluminescence Spectra. **J. Phys. Chem. B** 1041738-1745.

Nachtigallova, D., P. Nachtigall, M. Sierka and J. Sauer. 1999. Coordination and siting of Cu+ ions in ZSM-5: A combined quantum mechanics/interatomic potential function study. **Phys. Chem. Chem. Phys.** 1(8):2019-2026.

Neyman, K.M., P. Strodel, S.P. Ruzankin, N. Schlensog, H. Knoezinger and N. Roesch. 1995. N2 and CO molecules as probes of zeolite acidity: an infrared spectroscopy and density functional investigation. **Catal. Lett.** 31(2,3):273-285.

Ohba, T., H. Kanoh, K. Murata, M. Yudasaka, S. Iijima and K. Kaneko. 2002. Separation of adsorption isotherms of N2 in internal and interstitial nanopores of single-walled carbon nanohorn - A comparative study with experiment and simulation. **Stud. Surf. Sci. Catal.** 144(Characterization of Porous Solids VI):521-527.

Ono, Y., K. Osako, G.J. Kim and Y. Inoue. 1994. Ag-ZSM-5 as a catalyst for aromatization of alkanes, alkenes, and methanol. **Stud. Surf. Sci. Catal.** 84(ZEOLITES AND RELATED MICROPOROUS MATERIALS, PT. C):1773-1780.

Pan, W., X. Zhang, S. Li, D. Wu and Z. Mao. 2005. Measuring hydrogen storage capacity of carbon nanotubes by high-pressure microbalance. **Int. J. Hydrogen Energy** 30(7):719-722.

Perdew, J.P. 1986. Density-functional approximation for the correlation energy of the inhomogeneous electron gas. **Phys. Rev. B.** 338822–8824.

Pisani, C. and U. Birkenheuer. 1995. Embedded-cluster approach to the study of catalytic reactions in zeolite cavities. **Int. J. Quantum Chem., Quantum Chem. Symp.** 29(Atomic, Molecular, and Condensed Matter Theory and Computational Methods, Proceedings of the International Symposium, 1995):221-234.

Rappe, A.K., C.J. Casewit, K.S. Colwell, W.A. Goddard, III and W.M. Skiff. 1992. UFF, a full periodic table force field for molecular mechanics and molecular dynamics simulations. **J. Am. Chem. Soc.** 114(25):10024-10035.

Reed, A.E., L.A. Curtiss and F. Weinhold. 1988. Intermolecular interactions from a natural bond orbital, donor-acceptor viewpoint. **Chem. Rev.** 88(6):899-926.

Ricchiardi, G., A. de Man and J. Sauer. 2000. The effect of hydration on structure and location of Ti-sites in Ti-silicalite catalysts. A computational study. **Phys. Chem. Chem. Phys.** 2(10):2195-2204.

Rodriguez-Santiago, L., M. Sierka, V. Branchadell, M. Sodupe and J. Sauer. 1998. Coordination of Cu+ Ions to Zeolite Frameworks Strongly Enhances Their Ability to Bind NO2. An ab Initio Density Functional Study. **J. Am. Chem. Soc.** 120(7):1545-1551.

Rotkin, S.V. and I. Zharov. 2002. Nanotube light-controlled electronic switch. **Int. J. Nanosci.** 1(3-4):347-355.

Rozanska, X., R.A. van Santen, F. Hutschka and J. Hafner. 2001. A Periodic DFT Study of Intramolecular Isomerization Reactions of Toluene and Xylenes Catalyzed by Acidic Mordenite. **J. Am. Chem. Soc.** 123(31):7655-7667.

Ruggiero, C.E., S.M. Carrier, W.E. Antholine, J.W. Whittaker, C.J. Cramer and W.B. Tolman. 1993. Synthesis and structural and spectroscopic characterization of mononuclear copper nitrosyl complexes: models for nitric oxide adducts of copper proteins and copper-exchanged zeolites. **J. Am. Chem. Soc.** 115(24):11285-11298.

Ryder, J.A., A.K. Chakraborty and A.T. Bell. 2003. Density functional theory study of benzene oxidation over Fe-ZSM-5. **J. Catal.** 220(1):84-91.

Sato, S., Y. Yuu, H. Yahiro, N. Mizuno and M. Iwamoto. 1991. Cu-ZSM-5 zeolite as highly active catalyst for removal of nitrogen monoxide from emission of diesel engines. **App. Catal.** 70(1):L1-L5.

Sauer, J. and M. Sierka. 2000. Combining quantum mechanics and interatomic potential functions in ab initio studies of extended systems. **J. Comput. Chem.** 21(16):1470-1493.

Sauer, J., P. Ugliengo, E. Garrone and V.R. Saunders. 1994. Theoretical Study of van der Waals Complexes at Surface Sites in Comparison with the Experiment. **Chem. Rev.** 94(7):2095-2160.

Scarano, D., S. Bordiga, C. Lamberti, G. Spoto, G. Ricchiardi, A. Zecchina and C. Otero Arean. 1998. FTIR study of the interaction of CO with pure and silica-supported copper(I) oxide. **Surf. Sci.** 411(3):272-285.

Schneider, J.L., S.M. Carrier, C.E. Ruggiero, V.G. Young, Jr. and W.B. Tolman. 1998. Influences of Ligand Environment on the Spectroscopic Properties and Disproportionation Reactivity of Copper-Nitrosyl Complexes. **J. Am. Chem. Soc.** 120(44):11408-11418.

Schneider, W.F., K.C. Hass, R. Ramprasad and J.B. Adams. 1996. Cluster Models of Cu Binding and CO and NO Adsorption in Cu-Exchanged Zeolites. **J. Phys. Chem.** 100(15):6032-6046.

Senchenya, I.N., E. Garrone and P. Ugliengo. 1996. An ab initio study of terminal .scharw.SiOH and bridging .scharw.Si(OH)Al.rscharw.groups in zeolites and their interaction with carbon monoxide. **J. Mol. Struc. (THEOCHEM)** 368(1-3):93-110.

Shah, R., J.D. Gale and M.C. Payne. 1997. The active sites of microporous solid acid catalysts. **Phase Transitions** 61(1-4):67-81.

_____, M.C. Payne, M.H. Lee and J.D. Gale. 1996. Understanding the catalytic behavior of zeolites: a first-principles study of the adsorption of methanol. **Science** 271(5254):1395-1397.

Shenderova, O.A., B.L. Lawson, D. Areshkin and D.W. Brenner. 2001. Predicted structure and electronic properties of individual carbon nanocones and nanostructures assembled from nanocones. **Nanotechnology** 12(3):191-197.

Sierka, M. and J. Sauer. 2000. Finding transition structures in extended systems: A strategy based on a combined quantum mechanics-empirical valence bond approach. **J. Chem. Phys.** 112(16):6983-6996.

Sierka, M. and J. Sauer. 2001. Proton mobility in chabazite, faujasite, and ZSM-5 zeolite catalysts. Comparison based on ab initio calculations. **J. Phys. Chem. B** 105(8):1603-1613.

Sinclair, P.E., A. de Vries, P. Sherwood, C.R.A. Catlow and R.A. van Santen. 1998. Quantum-chemical studies of alkene chemisorption in chabazite: A comparison of cluster and embedded-cluster models. **J. Chem. Soc., Faraday Trans.** 94(22):3401-3408.

Soscun, H.J., P.J. O'Malley and A. Hinchliffe. 1995. An ab initio study of the molecular complexes formed between H2S and the acid sites of zeolites. **J. Mol. Struc. (THEOCHEM)** 341237-251.

Sotiropoulou, S. and N.A. Chaniotakis. 2003. Carbon nanotube array-based biosensor. **Anal. Bioanal. Chem.** 375(1):103-105.

Stefanovich, E.V. and T.N. Truong. 1998. A Simple Method for Incorporating Modeling Field Effects into Ab Initio Embedded Cluster Calculations of Crystals and Macromolecules. **J. Phys. Chem. B** 1023018-3022.

Svensson, M., S. Humbel, R.D.J. Froese, T. Matsubara, S. Sieber and K. Morokuma. 1996. ONIOM: A multilayered integrated MO + MM method for geometry optimization and single point predictions. A test for Diels-Alder reactions and $Pt(P(t\text{-}Bu)_3)_2 + H_2$ oxidative addition. **J. Phys. Chem.** 199619357.

Teunissen, E.H., A.P.J. Jansen, R.A. van Santen, R. Orlando and R. Dovesi. 1994a. Adsorption energies of NH3 and NH4+ in zeolites corrected for the long-range electrostatic potential of the crystal. **J. Chem. Phys.** 101(7):5865-5874.

_____, C. Roetti, C. Pisani, A.J.M.d. Man, A.P.J. Jansen, R. Orlando, R.A.v. Santen and R. Dovesi. 1994b. Proton transfer in zeolites: A comparison between cluster and crystal calculations. **Model. Simul. Mater. Sci. Eng.** 2(4):921-932.

Thiemens, M.H. and W.C. Trogler. 1991. Nylon production: an unknown source of atmospheric nitrous oxide. **Science** 251(4996):932-934.

Trout, B.L., A.K. Chakraborty and A.T. Bell. 1996. Local Spin Density Functional Theory Study of Copper Ion-Exchanged ZSM-5. **J. Phys. Chem.** 100(10):4173-4179.

Ugliengo, P., V.R. Saunders and E. Garrone. 1989. Silanol as a model for the free hydroxyl of amorphous silica: quantum-mechanical calculation of the interaction with carbon monoxide. **J. Phys. Chem.** 93(13):5210-5215.

Venuto, P.B. 1994. Organic catalysis over zeolites: a perspective on reaction paths within micropores. **Microporous Mater.** 2(5):297-411.

Vollmer, J.M., E.V. Stefanovich and T.N. Truong. 1999. Molecular Modeling of Interactions in Zeolites: An Ab Initio Embedded Cluster Study of NH3 Adsorption in Chabazite. **J. Phys. Chem. B** 103(44):9415-9422.

Vosko, S.H., L. Wilk and M. Nusair. 1980. Accurate spin-dependent electron liquid correlation energies for local spin density calculations: a critical analysis. **Can. J. Phys.** 58(8):1200-1211.

Warakulwit, C., S. Bamrungsap, P. Luksirikul, P. Khongpracha and J. Limtrakul. 2005. Diels-Alder cycloadditions of single-wall carbon nanotubes with electron-rich dienes: A theoretical study. **Stud. Surf. Sci. Catal.** 156(Nanoporous Materials IV):823-828.

Wohlstadter, J.N., J.L. Wilbur, G.B. Sigal, H.A. Biebuyck, M.A. Billadeau, L. Dong, A.B. Fischer, S.R. Gudibande, S.H. Jameison, J.H. Kenten, J. Leginus, J.K. Leland, R.J. Massey and S.J. Wohlstadter. 2003. Carbon nanotube-based biosensor. **Adv. Mater.** 15(14):1184-1187.

Yoshitake, T., Y. Shimakawa, S. Kuroshima, H. Kimura, T. Ichihashi, Y. Kubo, D. Kasuya, K. Takahashi, F. Kokai, M. Yudasaka and S. Iijima. 2002. Preparation of fine platinum catalyst supported on single-wall carbon nanohorns for fuel cell application. **Physica B: Condensed Matter** 323(1-4):124-126.

Zecchina, A., S. Bordiga, C. Lamberti, G. Spoto, L. Carnelli and C. Otero Arean. 1994. Low-Temperature Fourier Transform Infrared Study of the Interaction of CO with Cations in Alkali-Metal Exchanged ZSM-5 Zeolites. **J. Phys. Chem.** 98(38):9577-9582.

_____, C. Lamberti and S. Bordiga. 1998. Surface acidity and basicity. General concepts. **Catal. Today** 41(1-3):169-177.

_____ and C. Otero Arean. 1996. Diatomic molecular probes for mid-IR studies of zeolites. **Chem. Soc. Rev.** 25(3):187-197.

Zhanpeisov, N.U., W.S. Ju, M. Matsuoka and M. Anpo. 2003. Quantum Chemical Calculations on the Structure and Adsorption Properties of NO and N2O on Ag+ and Cu+ Ion-Exchanged Zeolites. **Structural Chemistry** 14(3):247-255.

_____, H. Nakatsuji, M. Hada, H. Nakai and M. Anpo. 1996. CO and NO adsorption on copper-containing zeolite. A theoretical ab initio study. **Catal. Lett.** 42(3,4):173-176.

Ziegler, T. 1991. Approximate Density Functional Theory as a Practical Tool in Molecular Energetics and Dynamics. **Chem. Rev.** 91(5):651-667.

Zygmunt, S.A., L.A. Curtiss, P. Zapol and L.E. Iton. 2000. Ab Initio and Density Functional Study of the Activation Barrier for Ethane Cracking in Cluster Models of Zeolite H-ZSM-5. **J. Phys. Chem. B** 104(9):1944-1949.